Biomass Conversion and Biorefinery (2024) 14:30667–30691
https://doi.org/10.1007/s13399-024-05441-4

ORIGINAL ARTICLE

Experimental and modeling studies on the removal of bromocresol green from aqueous solutions by using pine cone-derived activated biochar

Nihan Kaya[1] · **Zeynep Yıldız Uzun**[2]

Received: 5 October 2023 / Revised: 1 February 2024 / Accepted: 12 February 2024 / Published online: 29 February 2024

Abstract
This study was carried out to evaluate the potential application of pine cone (PC)-derived activated biochar which has a surface area of 1714.5 m^2/g for bromocresol green (BCG) dye removal from aqueous solution. Batch adsorption experiments involved varying pH, temperature, contact time, adsorbent dosage, and initial dye concentrations and the maximum BCG removal (96.27%) occurred at pH: 2.0, T: 45 °C, m: 2 g/L, t: 15 min., and C_o: 25 mg/L. To study the characteristics of adsorption, the adsorption kinetic isotherm and thermodynamic parameters were employed. The experimental data was evaluated to fit well with the Temkin isotherm ($R^2 = 0.99$) and the adsorption process followed pseudo-first-order kinetics ($R^2 = 0.96$). Thermodynamic parameters obtained from the adsorptive uptake showed that the interaction was endothermic and spontaneous in nature. The regenerated activated PC biochar showed good performance (95.0%), even, after 4th regeneration. To predict the BCG adsorption capacity of activated PC biochar, many different artificial neural network (ANN) models have been developed. The optimal ANN model gave mean absolute error (MAE), mean bias error (MBE), root mean square error (RMSE), and R^2 values of 0.036, 0.578, 0.947, and 0.999, respectively. The results obtained showed that ANN can be used to effectively model the BCG adsorption process.

Keywords Artificial neural network · Bromocresol green · Pine cone · Activated biochar · Pyrolysis · Adsorption

1 Introduction

One of the most important problems of the century we are in is the rapid decrease in clean water resources, the difficulty of access to water, and the increasing water poverty. Especially with rapid population growth, developing industry, increasing drought and excessive consumption, fresh water resources are rapidly depleting on a global scale. However, aquatic environments are mostly polluted due to factors arising from human activities and the threat of pollution continues to increase day by day [1]. Industrial sectors, including textiles, paper, cosmetics, paints, pharmaceuticals, plastics, and leather, stand as prominent contributors to environmental pollution, exerting a significant influence on the degradation of ecological balance [2, 3]. Dyestuffs, known for their resistance to biodegradation and prevalent presence in the wastewater of these industries, stand out as a significant organic pollutant. Without a reliable treatment method, the release of wastewater containing dyestuffs into receiving environments like lakes, rivers, seas, and oceans poses a severe toxicity threat to aquatic life and all organisms dependent on this water source [4, 5]. Textile wastewater, one of the most important environmental pollutants, is defined as wastewater with high volumes and large variations in composition. The high probability of containing non-biodegradable dyestuffs and toxic compounds brings the potential to pose a risk to the receiving waters. For this reason, it is of great importance to treat wastewater originating from textile industries with appropriate and effective methods [6]. Otherwise, the uncontrolled release of colored wastewater into the environment will lead to significant

✉ Nihan Kaya
nihan.kaya@omu.edu.tr; nihankaya44@gmail.com

Zeynep Yıldız Uzun
zyildiz@sinop.edu.tr

[1] Department of Chemical Engineering, Ondokuz Mayıs University, Engineering Faculty, Samsun, Turkey

[2] Boyabat Vocational School, Department of Chemistry and Chemical Processing Technologies, Sinop University, Sinop, Turkey

environmental issues, including the generation of toxic-carcinogenic aromatic amines in anaerobic conditions [7].

BCG is a dye from the triphenylmethane family, in other words, it is one of the triarylmethane dyes. Triarylmethane dyes are synthetic organic compounds containing triphenylmethane backbones. Triphenylmethane is a very easily oxidized substance, and when oxidized, it can take on different colors depending on the groups attached to the phenyl rings in its structure. Since most of the dyestuffs in this group are ionic, they can dissolve in water and can be classified as direct dyes according to their application. These compounds are quite intensely colored. BCG, one of the anionic dyes, is generally used as a pH indicator in applications such as growth media for microorganisms and titrations. Because in aqueous solution, at low pH, BCG ionizes and gives a mono-anionic form (yellow), while at high pH it becomes blue by giving dianionic form [8]. BCG has several applications in the medical field, including the measurement of serum albumin in blood tests and the detection of protein in urine samples. It is also used as a visual indicator in microbiology to determine the pH of bacterial growth media [9]. In addition, BCG is used in environmental monitoring to measure the pH of water samples and to determine the presence of acidic or alkaline pollutants. It can also be used as an analytical tool for the detection of certain chemicals, such as the detection of phosphate ions in soil samples. They are also widely used in textile industry for dyeing fibers such as wool, silk, nylon, and polyamide. Therefore, this anionic dyestuff containing sulfonic acid (-HSO_3) group is one of the organic pollutants frequently encountered in the textile wastewater [10].

Methods such as reverse osmosis, ion exchange, and chemical oxidation are widely used technologies for wastewater treatment. However, since these methods cause the release of toxic secondary pollutants in the ecosystem, the use of these methods in industrial wastewater treatment is limited. For this reason, the most effective and economically applicable method for removing organic substances that are difficult or impossible to biodegrade, such as dyestuff, from wastewater is undoubtedly the adsorption process [11, 12]. Adsorption is considered to be superior to other techniques due to its low cost, simplicity of design, high efficiency, and ability to separate a wide variety of chemical compounds. The adsorption process is affected by many physico-chemical factors such as dye/sorbent interaction, surface area of the adsorbent, particle size, temperature, pH, and contact time [13]. Many different types of adsorbents are used in the adsorption process. Among them, activated carbon is most commonly used in wastewater treatment. However, its high cost limits its use. Due to this disadvantage, adsorbents obtained from natural, industrial, and agricultural wastes, which can be an alternative to activated carbon, have been preferred in recent years. These adsorbers draw attention due to their low cost, efficiency in pollution removal, and not leaving harmful or toxic substances to the environment after adsorption [14].

Since activated carbon is used not only in water treatment but also in many industrial areas, its importance is increasing day by day. Therefore, the synthesis of low-cost activated carbon from different starting materials has gained great importance in recent years. In the past, activated carbon synthesis was generally produced from materials such as coal, coal derivatives, animal fossils, and cellulosic raw materials (wood, etc.) [15]. Today, these materials have started to be used in different sectors depending on the increasing world population and energy needs. For this reason, the raw materials used in the synthesis of activated carbon showed differences. The raw materials used in the synthesis are generally started to be obtained from waste materials, especially from biomass-based materials. In this way, as it provides benefits both economically and in terms of renewability, its preference as raw material has increased. Biomass can be defined as all organic matter that can be renewed in less than a century, including plants growing on land and in water, animal waste, food industry wastes and forest products, and urban waste. The main component of biomass is carbohydrate polymers and oligomers (65–75%) that have high molar mass, and lignin (18–35%). In addition, there are mostly organic extractives and inorganic substances (4–10%) that have low molar mass in its structure [16, 17]. In particular, woody biomass such as agricultural residues and forest wastes are widely used as they are easily available compared to other raw materials. The pine cone (PC) used as biomass in this study is the female flower of the pine and is found in forests as waste in large quantities. PC, which is mainly composed of lignin, cellulose, hemicellulose, resin and tannin, is a cheap and abundant forest product [18]. PCs which were used as precursors were harvested from central part of Anatolia in Turkey.

PCs are a natural part of forest ecosystems, because of they are a renewable resource as pine trees continually produce cones as part of their life cycle, and their presence is not harmful. When their accumulation becomes excessive or if there are other environmental factors in play (such as drought conditions) that issues may arise. Especially, in regions prone to wildfires, a large accumulation of dry PCs on the ground can potentially increase the risk of fire. During periods of dry weather, PCs can become highly flammable. Therefore, by converting PCs into biochar in this study, we aim to utilize waste materials effectively, contributing to a more sustainable and environmentally friendly approach. Pine trees are widespread in many regions, making PCs a locally available and abundant resource. Specific statistics on PC quantities may vary depending on factors such as location, species of pine, and environmental conditions. In Turkey, Communiqué No. 283, which regulates forest production, states that a maximum of 100–120 kg

(approximately 300 pieces) of cones can be obtained from a pine tree between 20 and 80 years old [19]. This can reduce the need for transporting feedstock over long distances, contributing to a more localized and sustainable biochar production system. For these reasons, the production of biochar from PCs which are a byproduct of forestry and landscaping activities is an area of research that shows promise in terms of sustainable waste utilization, and aligns with the principles of sustainable resource management.

The pyrolysis of biomass is the main technique used to produce biochar. Pyrolysis is a process that thermally decomposes biomass by heating it at high temperatures in a controlled environment, i.e., under an atmosphere of inert gas such as N_2, or atmosphere containing limited amount of O_2. This process starts at 350–550 °C and continues until 700–800 °C. During pyrolysis, the volatile organic components in the biomass are thermally decomposed to release a vapor phase, leaving the solid phase called biochar. Which of the solid, liquid, or gaseous products obtained in pyrolysis process will have the highest yield depends on the type of biomass, process parameters, and also reactor type [20]. Slow pyrolysis is often preferred for producing biochar because the highest solids yield is achieved by slow pyrolysis (35–50% by weight). This process is carried out at temperatures between 300 and 800 °C with heating rates of 5–10 °C/min [21]. The composition of the solid product obtained as a result of this process, which supports biochar production, becomes carbon-rich compared to oxygen and hydrogen, approaching the composition of coal. This carbon-rich material commonly used in soil amendment, carbon sequestration, and environmental remediation due to its ability to improve soil fertility, retain water, and reduce greenhouse gas emissions.

Activation of biochar after carbonization is generally a process to further increase the porosity of biochar, but this process can also change the surface chemistry of the biochar. The activation process is usually done after biochar production. Many different activation methods are used to activate biochar successfully, and these methods can be classified as physical activation and chemical activation in the most general form. In both cases, the material is thermally treated in an activating agent environment. The type of activator helps us determine whether the method is physical or chemical. In chemical activation uses different chemical agents, usually in solid or liquid form, to activate the biochar through dehydration and oxidation reactions. Chemical activation can be applied directly to the biomass to produce the activated biochar or to the biochar after pyrolysis. Chemical activation is carried out at higher temperatures than physical activation and is more expensive. However, with this process, biochar products with higher surface area values are obtained and higher activation efficiency is achieved. There are many chemical activating agents used for activation. Among these, KOH, NaOH, NH_3, K_2CO_3, and $ZnCl_2$, which are alkaline, and HNO_3, H_3PO_4, and H_2SO_4, which are acidic, stand out. Among them, KOH is particularly effective in creating micropores and increasing the specific surface area [22]. The importance of chemical activation lies in the fact that it improves the functionality of biochar and makes it more suitable for various applications. For example, activated biochar can be used in wastewater treatment to remove pollutants such as heavy metals, organic compounds, and nutrients. It can also be used as a catalyst in chemical reactions or as a sorbent in gas purification processes. In addition, chemical activation of biochar can increase its economic value, making it a viable option for waste management and renewable energy production.

In recent years, modeling and simulation studies, which has been used to obtain more information about process conditions, have gained great importance. Especially, % removal is very important in adsorption processes. Studies carried out on non-optimized systems may result in longer times with the use of more chemicals. Therefore, modeling of different parameters is important to estimate the target such as removal percentage in adsorption processes [23]. Recently, artificial neural networks (ANN) method has been successfully applied in modeling adsorption systems. ANN is a preferred method in solving complex and multidimensional functional relationships by using the information obtained from experimental data. In literature, several researchers have modeled the adsorption of different types of pollutants with artificial neural networks [24–26]. For example, Prasad and Yadav (2020) created an artificial neural network model to predict methylene blue adsorption [27]. In another study, Praveen et al. (2021) used an artificial neural network to model the adsorption of cationic dye Basic Violet 03 using biochar produced from groundnut hull [26].

BCG dye finds wide application areas in laboratories and various industries; however, its presence in water resources raises concerns due to potential toxic effects on aquatic organisms and health risks to humans. Especially, the threat it poses to ecosystems underscores the need for employing low-cost adsorbents derived from biomass in BCG removal. This necessity stems from considerations of cost-effectiveness, accessibility, and environmental sustainability. This study focuses on two key aspects: batch-mode adsorption of BCG from aqueous solutions using activated PC biochar and modeling the removal process using the ANN method. The inclusion of ANN adds a novel dimension to the study, particularly enhancing its comprehensiveness. The application of ANN proves especially valuable in water treatment scenarios where understanding and optimizing the removal efficiency of contaminants is crucial. This is because using ANN for removal modeling enables the capture of intricate relationships

between input variables and removal efficiency, even in situations where the underlying mechanisms are not fully understood.

In this study, biochar with high porosity and surface area was obtained by using lignocellulosic PC biomass as a raw material, which is one of the forest wastes, by performing pyrolysis and activation processes together. The obtained product was used as an adsorbent in the removal of BCG dye from aqueous solution. The effects of various adsorption parameters such as temperature, pH, initial dye concentration, contact time, and adsorbent dosage on the adsorption capacity of this KOH-activated biochar product were investigated. In addition, the kinetic and thermodynamic parameters of the adsorption process were also determined. The prediction of the BCG adsorption capacity of the activated biochar was modeled using an artificial neural network.

2 Material and methods

2.1 Material

BCG dyestuff was chosen as a representative model pollutant owing to its potential environmental risk. Procured from Sigma-Aldrich, the dyestuff was of analytical grade and employed without additional purification. Comprehensive details regarding the dyestuff can be found in Table 1.

2.2 Preparation and characterization of pine cone-derived activated biochar

The PCs used in the study were collected from Ankara, Turkey, and were used without any pre-cleaning process. Firstly, the dried and reduced size raw PCs were subjected to sieve analysis, and those with particle sizes smaller than 250 µm

Table 1 Characteristic properties of BCG dye

Dyestuff	Reactive Green 15
IUPAC Name	2,6-dibromo-4-[3-(3,5-dibromo-4-hydroxy-2-methylphenyl)-1,1-dioxo-2,1λ^6-benzoxathiol-3-yl]-3-methylphenol
Commercial Name	Bromocresol Green
CAS Number	76-60-8
Appearance	Beige to brown powder
Empirical Formula	$C_{21}H_{14}Br_4O_5S$
Molecular Weight	698.02 g/mol
3D Molecular Structure	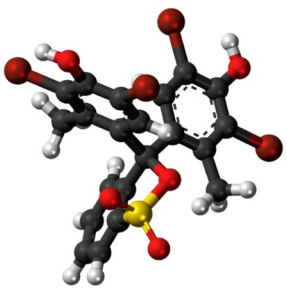
Chemical Structure	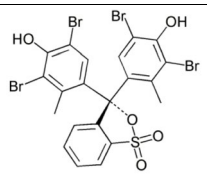
λ_{max}	pH=3.8 (Yellow) → 460 nm pH=5.4 (Blue) → 615 m

were used in the preparation of biochar. A stainless steel blade mill (Waring, USA) was used to reduce the size of the dried PC samples.

The pyrolysis and activation procedures necessary for the production of activated PC biochar were conducted independently. Firstly, PCs were pyrolyzed for 1 h at a temperature of 600 °C, 10 °C/min heating rate, and 100 mL/min N_2 flow rate in an electrically heated cylindrical furnace. Then, the carbonized solid product (biochar) was impregnated using 1 M KOH solution at impregnation (by weight) ratio of 1:4 (biochar/KOH solution). Activation was carried out at the same heating rate (10 °C/min) and inert gas (N_2) flow rate at a temperature of 800 °C for 1 h [28]. Finally, activated biochar was neutralized/purified and dried for using in adsorption experiments. To achieve this objective, the generated activated PC biochar underwent washing in 0.5 M HCl solution with agitation at room temperature, followed by rinsing with deionized water until the washings reached a neutral pH. Subsequently, the samples were dried in an oven at 105 °C for 24 h.

The surface functional groups of PC derived activated biochar (PC-AB) before and after adsorption process were evaluated using Perkin Elmer-Spectrum Two FT-IR spectrometer (USA). Spectra were recorded in a wavelength range of 600–4000 cm^{-1} at room temperature with spectral resolution 4 cm^{-1}. SEM device (ZEISS/LEO EVO 40, USA) was used to investigate the surface morphology of PC-AB used as an adsorbent before and after adsorption process. The elemental composition of PC-AB was obtained using energy dispersive X-ray spectrometer (JEOL JSM-7001F, USA).

2.3 Determination of effectiveness of PC-AB in removal of BCG dye from aqueous solution

Adsorption experiments were carried out using a batch mode. The stock aqueous solution of BCG was prepared at a concentration of 1000 mg/L. Standard solutions (1–50 mg/L) and working solutions (25–100 mg/L) were prepared from stock solution by dilution with deionized water. The initial pH of the working solution was approximately 6.27. BCG solutions underwent pH adjustment using 0.1 M NaOH and 0.1 M HCl solutions. Various parameters influencing the adsorption process, including pH (2–10), adsorbent dosage (0.1–0.5 g/250 mL solution), and temperature (25–45 °C), were investigated under consistent stirring at 150 rpm in water bath. During the adsorption process, samples were systematically collected at pre-established time intervals. Specifically, samples were gathered at intervals of every 3 min, following which the adsorbent was separated from the samples via filtration. The residual BCG dye concentration was determined using a UV–Visible Spectrophotometer (DR2400, Hach Company, USA). Spectrophotometric measurements were conducted at a wavelength (λ_{max}) suitable for the color of the initial working solution (Table 1). The amount of BCG dye adsorbed per unit mass of the adsorbent (q_e) at equilibrium was calculated according to the following Eq. (1) and the percentage of BCG dye removed was calculated by using the Eq. (2) [29].

$$q_e = \left(C_0 - C_e\right) \times \frac{V}{m} \tag{1}$$

$$\text{BCG dye removal (\%)} = \frac{C_0 - C_e}{C_0} \times 100 \tag{2}$$

where q_e is the amount of adsorbed dye per gram of adsorbent in equilibrium (mg/g), C_o and C_e are the initial and final dye concentration in solution phase, respectively (mg/L), V is the volume of dye solution (L), and m is the weight of adsorbent (g). To guarantee result reproducibility, the adsorption experiments were conducted three times using carefully prepared control solutions under consistent experimental conditions. The average values derived from these trials were employed in data analysis, revealing relative standard deviations within a range of ± 1.0%.

2.4 Artificial neural network modeling of BCG adsorption onto PC-AB

Artificial neural network models (ANN) are a set of data-driven models that are based on exploring relationships with target values using a set of input arguments and are used for output prediction. Among many ANN architectures, the feed forward back propagation network was chosen in this study. This architecture is reported to be suitable for pattern matching and pattern predictive problems in literature [30]. The general architecture of the model consists of an input layer, a hidden layer and an output layer. Figure 1 represents a network with 5 input variables, 7 hidden layers with 15 neurons, and an output layer with 1 neuron in this study. In Feed forward back propagation network, every neuron in each layer is connected unidirectionally, where the weighted total input is combined with a bias, then goes through a transfer function to generate an output without feedback to input neurons.

Statistical parameters are used to evaluate the performance of the developed ANN model in literature. These parameters are; root mean square error (RMSE), mean absolute error (MAE), mean bias error (MBE) and correlation coefficient R^2 of each ANN structure (Eqs. 3–5) [31, 32].

$$\text{RMSE} = \sqrt{\frac{1}{N}\sum_{i=1}^{N}\left(H_i - H_{i,\text{model}}\right)^2} \tag{3}$$

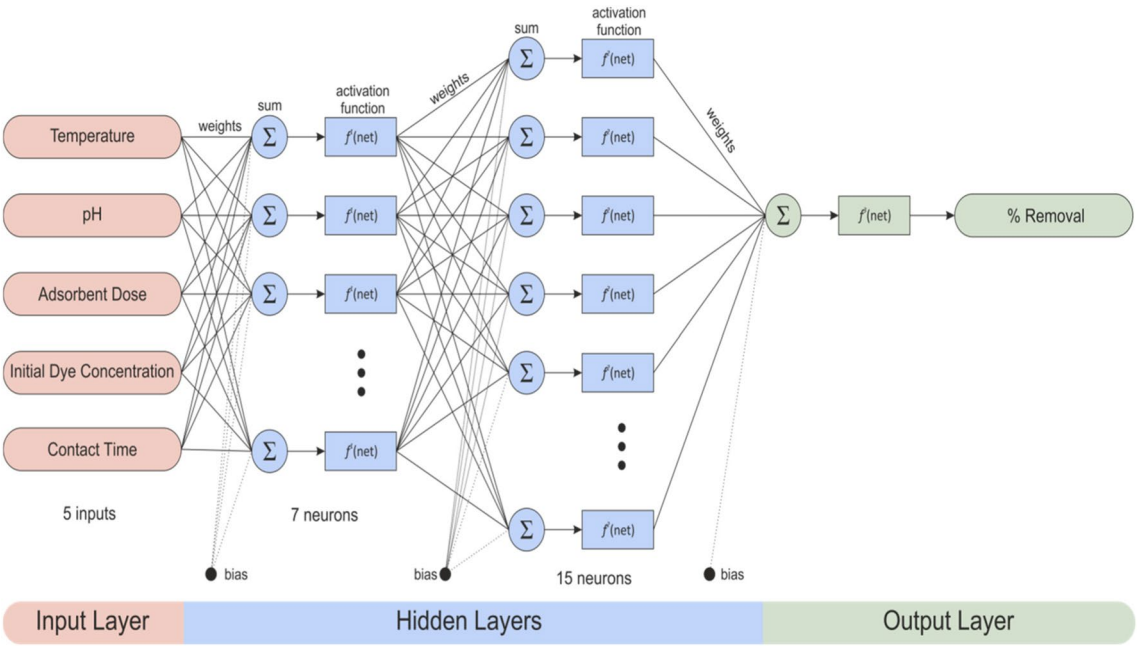

Fig. 1 Artificial neural network structure applied in this work

$$\mathrm{MAE} = \frac{1}{N}\sum_{i=1}^{N}\left|H_i - H_{i,\mathrm{model}}\right| \tag{4}$$

$$\mathrm{MBE} = \frac{1}{N}\sum_{i=1}^{N}\left(H_i - H_{i,\mathrm{model}}\right) \tag{5}$$

In these equations, N is the number of samples, H_i is the actual value of the percentage of BCG removal, and $H_{i,\mathrm{model}}$ is the predicted value of the percentage of BCG removal. In this research, we employed a range of variable parameters during the adsorption experiments, including temperature, pH, adsorbent dosage, initial dye concentration, and contact time. These parameters were subsequently utilized as input variables for modeling the adsorption process through artificial neural networks. Our objective during the modeling phase was to maximize the percentage of BCG removal (% BCG removal), which we designated as the primary estimation parameter and set as the system's output.

2.5 Regeneration of adsorbent

In this study, we conducted an analysis to assess the reusability of activated PC biochar and evaluate its effectiveness as an adsorbent. Initially, following the completion of the adsorption process, 0.5 g PC-AB loaded with BCG underwent a sequential treatment involving absolute ethanol (50 mL) for 1 h, followed by deionized water, as outlined by Khan et al. in their 2018 study [33]. These straightforward procedures effectively washed out the adsorbed BCG and regenerated the PC-AB material. Spectrophotometric analysis revealed a remarkable desorption efficiency of 99%. The regenerated adsorbent was dried under the same conditions before being used again.

3 Results and discussion

PCs, which are the reproductive structures of pine trees, can be a suitable source of biomass for biochar production. PCs contain lignocellulose, a complex material composed of cellulose (35–55%), hemicellulose (20–40%), and lignin (10–25%), which are the building blocks of plant cells [34]. Lignocellulose is a rich source of carbon and can be converted into biochar through pyrolysis [35]. Upon reviewing the thermogravimetric analysis data from the 2021 study conducted by Kaya and Yıldız Uzun, it is evident that the decomposition of PC proceeds in three distinct steps. The initial decomposition transpires between 27 and 113 °C, during which the removal of moisture and low molecular weight substances from the surface is noted. The main decomposition of PC, consist of the second and third degradation steps, unfolds in the temperature range of 205–468 °C. The significant mass loss observed in this phase is attributed to the decomposition of hemicellulose, cellulose, and lignin. Based on the proximate analysis results, the PCs were found to have low ash content (3.2%), high volatile matter content (72%), and a fixed carbon content of 24.8%. Furthermore, elemental analysis indicated that the biomass had high carbon (44.75%) and hydrogen (5.37%) content [36]. Considering that the main characteristics of the raw materials to be

used to obtain porous biochar should be high carbon content and low inorganic matter (ash content), it is thought that low cost PCs, which can be found everywhere can be an excellent precursor.

Through the pyrolysis of PCs employed as the biomass source in this investigation, a carbon-rich material was derived by eliminating volatile organic compounds and moisture from the structure. The surface area of activated PC biochar obtained by chemical activation of this product was determined through nitrogen adsorption analyses. The experimental adsorption data was analyzed using the Brunauer-Emmet-Teller (BET) method to calculate the surface area. The resulting measurements for the BET surface area and pore volume of the activated biochar product were 1714.5 m^2/g and 0.684 cm^3/g, respectively [28]. Comparing the high surface area value achieved through activation to the surface area of PC biochar prepared without activation under similar conditions (259.74 m^2/g) revealed notable enhancements [37]. To clarify, the activation process led to a 6.6-fold increase in surface area. This enhancement not only improved pore volume but also improved pore size distribution, enabling the production of a cost-effective and eco-friendly adsorbent. These improvements were distinctly evident through the activation process. Especially, alkaline modification of biochar, involving chemical reduction with a reducing agent such as KOH, improved the porosity and specific surface area of the biochar by removing the non-pyrolysed organic matter and ash content from the pores. As a result, KOH activation was an important process in the production of PC biochar because it enhanced the properties of the material, made it suitable for various applications. However, in general, the activation process typically involves opening up pores and increasing the surface area of the biochar, leading to improved adsorption capabilities. Increased surface area, improved pore size distribution, and surface functional groups are some ways in which the adsorption capacity of biochars can change with chemical activation. But it is important to note that the specific impact of chemical activation on adsorption capacity can vary based on the type of biochar, the activating agent, and the activation conditions employed.

The use of carbon-based materials as adsorbents is a promising area of research with many potential applications in environmental, industrial, and biomedical fields. They have several advantages, including their high selectivity for certain types of molecules, their ability to be regenerated and reused, and their low cost compared to other types of adsorbents. The adsorption capacity of these materials depends on factors such as the surface area, pore size distribution, and also chemical composition of the adsorbent [38]. In this context, the elemental composition of the activated PC biochar especially carbon content of the sample was obtained using energy dispersive X-ray spectrometer. In other words, this technique was used to identify the elemental composition of the material, including the concentration of carbon, oxygen, and other elements. Figure 2 shows the EDX spectra of activated PC biochar, indicating a weight fraction of 89.9% carbon which is confirmed by the sharp carbon peaks. In other words, the EDX mapping indicated the carbon-rich areas in the structure. The EDX analysis results indicated that the activated biochar sample had a high abundance of carbon, making it a suitable alternative adsorbent to commercially available, expensive activated carbon. The percentage of carbon in commercial activated carbon can vary depending on the source material and the manufacturing process. Generally, commercial activated carbon contains a high percentage of carbon, often ranging from 80 to 95% or more. The remaining percentage typically consists of ash and other impurities. The surface area is in the range of 400–1000 m^2/g and grain size usually less than 0.18 mm (for powdered activated carbon) or in the range of 0.2–5 mm (for granular activated carbon) [39, 40]. With the EDX analysis, it is clearly seen that the volatile carbon in its structure is removed from the pores by alkali modification of the PC biochar and thus the fixed carbon content in the biochar increases.

3.1 Adsorption of BCG onto activated PC biochar

BCG is a pH-sensitive dye that changes color based on the acidity or alkalinity of a solution. BCG adsorption has practical applications in various fields, including water treatment, environmental remediation, and pharmaceutical industry. The process can be used to remove BCG from contaminated solutions or to isolate the dye for analytical purposes. The efficiency of the adsorption process is influenced by several factors such as the surface area, pore size distribution, chemical composition, and surface charge of the adsorbent. In addition, the concentration of BCG in the solution, contact time, temperature, and pH of the solution can also affect the adsorption capacity.

3.1.1 Effect of initial solution pH

The effect of initial solution pH on the adsorption process depends on the charge characteristics of the adsorbent and the adsorbate. The pH can affect the surface charge of the adsorbent, as well as the net charge of the adsorbate, leading to changes in the adsorption capacity and selectivity. Therefore, it is important to consider the initial solution pH when designing and optimizing adsorption processes. Therefore, the effect of solution pH on the adsorption of BCG onto PC-AB was studied in the pH range of 2–10. The removal efficiency of BCG is shown in Fig. 3.

As can be seen from the figure, the maximum removal efficiency was found to be 94.76% at pH 2.0. It would be

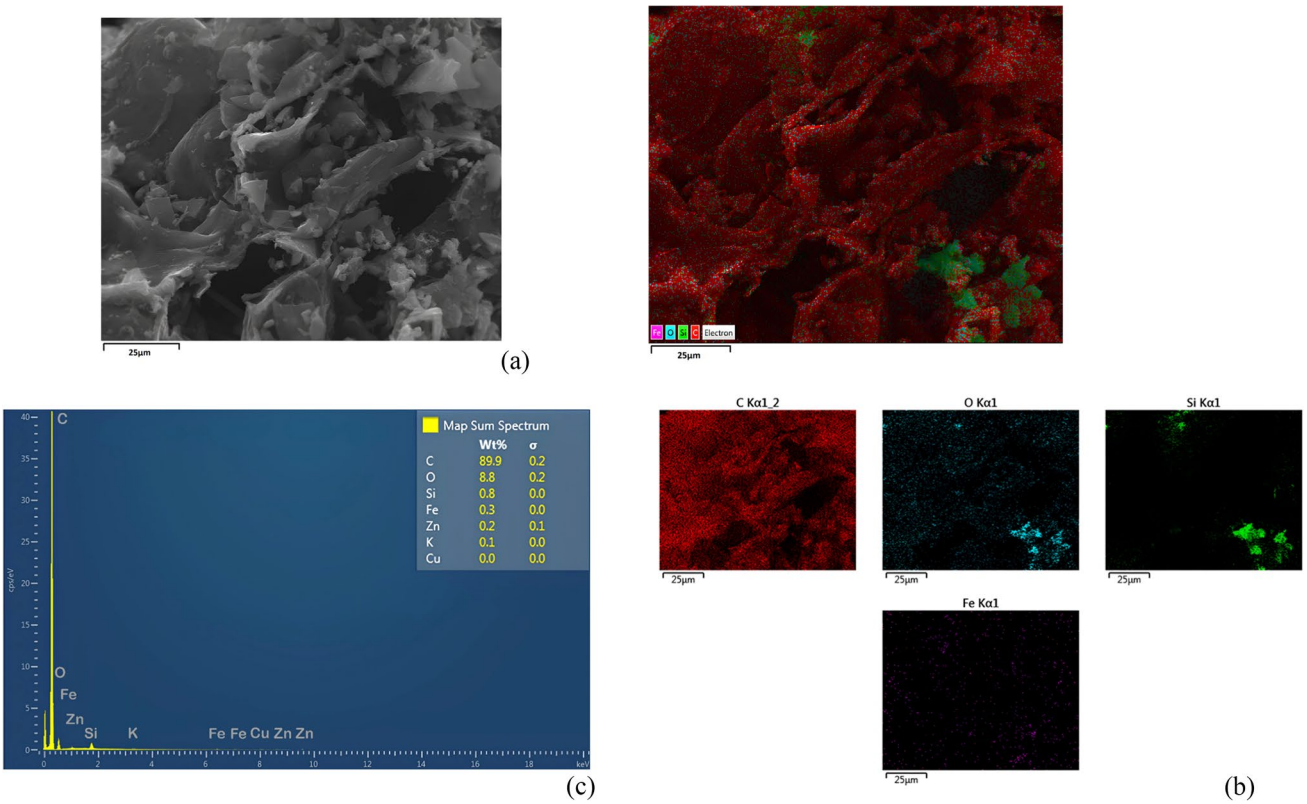

Fig. 2 EDX mapping of activated PC biochar. **a** Electron image. **b** Layered image. **c** EDX spectra

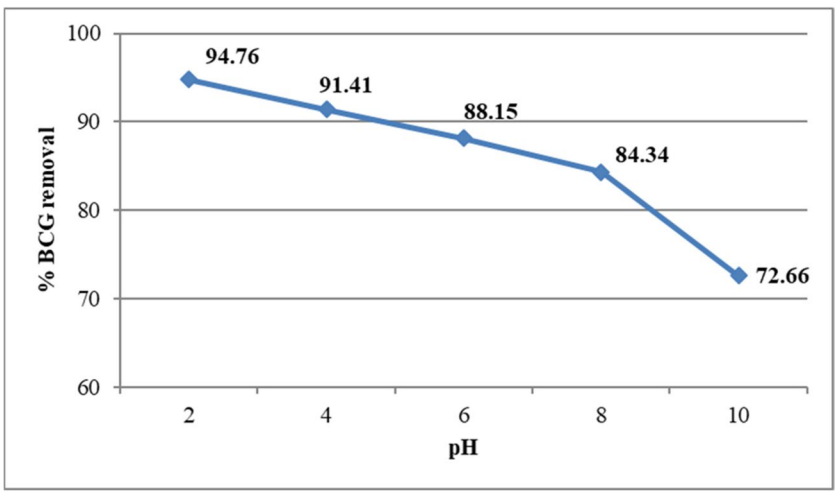

Fig. 3 The removal efficiencies (%) achieved in the adsorption of BCG from aqueous solutions at different pH values (C_0 = 25 mg/L; adsorbent dosage = 0.5 g/250 mL solution; T = 25 °C)

more accurate to explain this result by considering the isoelectric point of the adsorbent. The point of zero charge (pzc) is the pH value at which a solid material, such as a mineral or an adsorbent, has no net electric charge on its surface. At this pH value, the surface of the material is neither positively nor negatively charged, and its behavior with respect to adsorption, ion exchange, and other surface reactions can change dramatically. The pzc is determined by measuring the surface charge density of the material at different pH values and determining the pH value at which the surface charge density is zero [41]. Above the pzc, the surface of the material carries a net negative charge and attracts positively charged ions, while below the pzc, the surface carries a net positive charge and attracts negatively charged ions [42]. Experimental results have shown that, as the solution pH droped below pH 5.2, which was the isoelectric value of

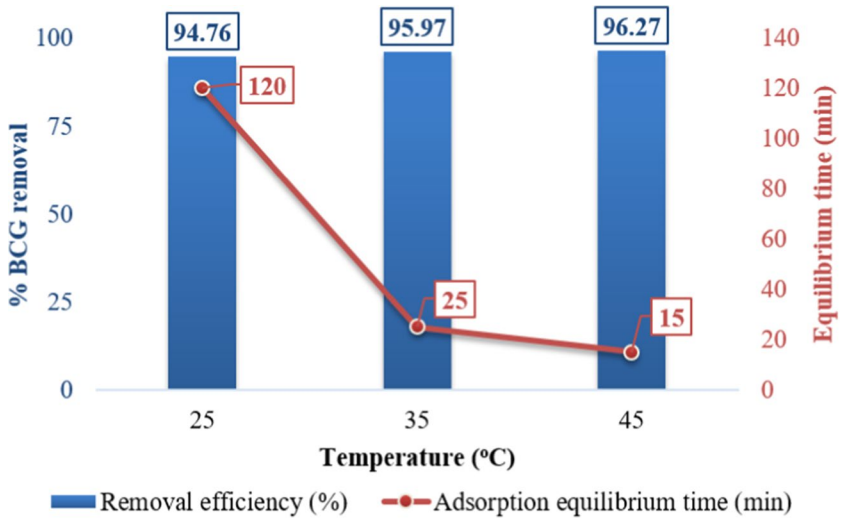

Fig. 4 The removal efficiencies (%) achieved in the adsorption of BCG dye from aqueous solutions at different temperature values (C_0 = 25 mg/L; adsorbent dosage = 0.5 g/250 mL solution; pH = 2)

PC-AB, the adsorbent surface became positively charged [28]. Thus, the anionic BCG dye, which existed in the form of negatively charged ions in aqueous solution, was adhere sufficiently to the adsorbent surface due to the electrostatic interaction between the dye molecules and the adsorbent surface at low pH values. Also, due to the adsorbent surface had a net positive charge, it was protonated at low pH values such as pH 2.0 and the surface charge became even more positive. This resulted in stronger electrostatic attraction between the surface and the adsorbate, improving the adsorption process. Thereby, the removal efficiency increased due to a strong ionic interaction between the BCG molecules with PC-AB surface at pH 2.0 [43]. In general, besides electrostatic interactions, there are several other mechanisms such as Van der Waals forces, dipole–dipole interactions, hydrogen bonding, and pore-filling or intrapore diffusion involved in adsorption processes. The relative importance of these mechanisms depends on factors such as the nature of the adsorbent and adsorbate, temperature, pressure, and the specific conditions of the adsorption process. The combination of these mechanisms often contributes to the overall adsorption behavior observed in different systems. However, electrostatic interactions play a crucial role in adsorption processes, particularly when charged species are involved [44]. In the adsorption of BCG dye, since the surfaces of both the adsorbent and the adsorbate are charged depending on the pH of the solution, electrostatic repulsion and attraction forces between the charged surfaces played a more effective role than other adsorption mechanisms [45]. As a result, the effect of initial solution pH on the adsorption process can be explained by considering the charge characteristics of the adsorbent and the adsorbate. At low pH values, the solution is acidic, which means that the concentration of hydrogen ions (H^+) is high. These hydrogen ions can interact with the functional groups on the adsorbent surface, leading to protonation of the surface groups. This can change the charge characteristics of the surface and affect the adsorption process. Experimental results show that anionic dyes containing sulfonate ions (SO_3^-) such as BCG can be adsorbed on positively charged adsorbents.

3.1.2 Effect of temperature

Temperature can have a significant effect on the adsorption process, which is the process by which molecules or ions are attracted and bound to the surface of a solid material, such as an adsorbent. The effect of temperature on adsorption depends on several factors, including the type of adsorbent and adsorbate, the chemical and physical properties of the adsorbate, and the conditions of the system. In general, increasing the temperature can increase the rate of adsorption, especially for chemisorption or strongly-bound adsorbates, because higher temperatures provide more energy for the adsorbate molecules to move and overcome the attractive forces holding them in solution [46]. However, for physisorption or weakly-bound adsorbates, increasing temperature may decrease adsorption rates because it can disrupt the chemical bonds or weak interactions between the adsorbate and adsorbent surface [47]. Moreover, the thermodynamic stability of the adsorbed species can also be affected by temperature. At higher temperatures, the adsorbed species may become less stable and may desorb from the adsorbent surface, leading to a decrease in adsorption capacity. However, in some cases, the adsorption capacity may increase with temperature due to changes in the surface chemistry or structure of the adsorbent. As a result, the effect of temperature on the adsorption process can be complex and depends on the specific conditions and materials involved. Therefore, it is important to carefully study and optimize the temperature conditions to achieve the desired adsorption performance. In this study, the % adsorption efficiencies achieved in the removal of BCG dyestuff from aqueous solutions at three

different temperature values by using activated biochar obtained from PC are given in Fig. 4.

As seen in Fig. 4, the efficiency of adsorption tends to increase with increasing temperature. This is because an increase in temperature provides more thermal energy to the BCG molecules, allowing them to overcome the attractive forces holding them together in the liquid phase and move toward the surface of the adsorbent. Especially, as the temperature increased, the kinetic energy of the BCG molecules also increased, making them more likely to collide with the surface of the adsorbent and become adsorbed. This increased mobility and collision frequency enhanced the adsorption process and led to a higher magnitude of adsorption (96.27%) in a shorter time. In this way, it was possible to reach equilibrium in a much shorter time in the adsorption system, especially at high temperatures. Although the temperature increase did not cause a significant increase in the efficiency of the BCG removal process, it positively affected the equilibrium time in the adsorption process and reduced the adsorption time from 120 to 15 min. An increase in adsorption capacity with rising temperature suggested that the process was chemical in nature. Consequently, experimental results showed that BCG removal was an endothermic process.

3.1.3 Effect of initial dye concentration and adsorbent dosage

The initial adsorbate concentration is an important factor in determining the adsorption capacity, rate, equilibrium concentration, and efficiency of the adsorption process. Therefore, it is important to carefully consider and optimize the initial adsorbate concentration to achieve the desired level of adsorption efficiency. Therefore, in this part of the study, batch adsorption experiments were carried out by keeping the pH, temperature, and amount of adsorbent constant, changing only the initial concentrations of the BCG solutions. The % adsorption efficiency and adsorption capacity values reached at different initial BCG concentration values by using the activated biochar obtained from PC as an adsorbent are given in Fig. 5.

From Fig. 5, it is clearly seen that by changing the initial BCG concentration in the range of 25–100 mg/L, the % adsorption efficiency decreases, whereas the adsorption capacity values increase [48]. At high initial concentrations, the efficiency of the adsorption process decreased due to the saturation of the active adsorption sites on the adsorbent surface, leading to incomplete removal of the adsorbate. Therefore, with increasing initial concentration, the BCG removal efficiency decreased from 96.27 to 80.49%. At the same time, as the initial adsorbate concentration increased, the adsorption capacity of the PC-AB increased. This was because a higher concentration of BCG molecules means more molecules were available to be adsorbed onto the adsorbent surface, resulting in a higher adsorption capacity. In other words, this result can be explained by increasing the initial concentration of the adsorbate, increasing the driving force required for mass transfer and thus increasing the adsorption capacity. The initial adsorbate concentration also affected the rate at which adsorption occured. At low initial concentrations, the rate of adsorption was generally higher as there were more available sites on the adsorbent surface for adsorption. Experimental results showed that the BCG adsorption process performed at an initial concentration of 25 mg/L was completed within 15 min and reached equilibrium. However, at high initial concentrations, the adsorption rate decreased due to the saturation of the available adsorption sites. The time to reach equilibrium increased to 80 min.The equilibrium concentration of the adsorbate was also affected by the initial adsorbate concentration. At low initial concentrations, the equilibrium concentration was generally lower due to the higher adsorption efficiency. However, at high initial concentrations, the equilibrium concentration reached higher values with the decrease of the

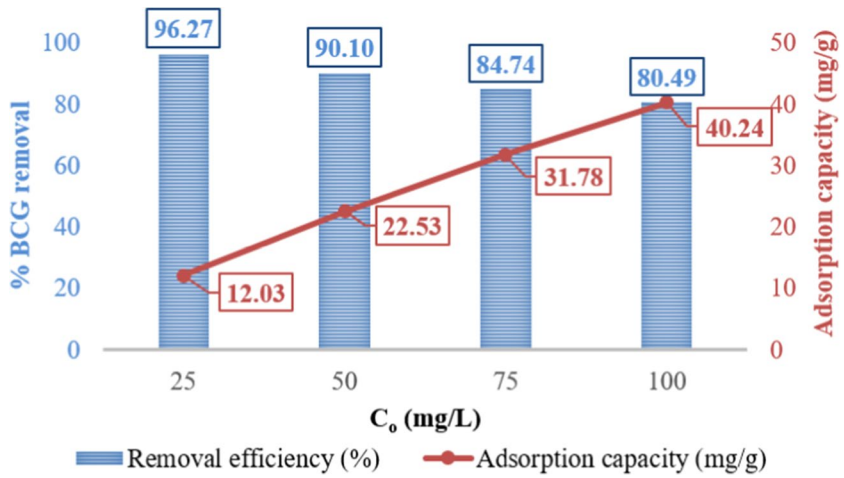

Fig. 5 The % removal efficiency and adsorption capacity values reached at different initial BCG concentration values (pH = 2, adsorbent amount = 0.5 g/250 mL solution; T = 45 °C)

adsorption efficiency due to the saturation of the existing adsorption sites.

The adsorbent dosage is also very important factor in determining the adsorption capacity, rate, equilibrium time, and efficiency of the adsorption process as is the initial adsorbate concentration. The % adsorption efficiencies and adsorption capacity values achieved in the removal of BCG dyestuff from aqueous solutions at different adsorbent amount by using activated biochar obtained from PC as an adsorbent are given in Fig. 6.

As can be seen in Fig. 6, the efficiency of the adsorption process increased from 77.48 to 96.27% with increasing adsorbent dose in the range of 0.1–0.5 g. This is because the increase in adsorbent dosage leads to an increase in the number of active adsorption sites available, which increases the adsorption process and speed. In the batch adsorption experiments carried out, 0.5 g of adsorbent is accepted and since an effective removal efficiency was achieved, this value was not exceeded in the studies. Especially as can be seen from the literature, beyond a certain point, the adsorption process can be limited by other factors such as mass transfer resistance, which may cause a decrease in efficiency. For this reason, pollutant removal efficiency may plateau or even decrease above a certain limit value. For this reason, the optimized adsorbent amount was determined as 0.5 g to achieve the desired adsorption efficiency [49]. As the adsorbent dose increased, providing more usable effective adsorption sites for the adhesion of BCG molecules increased not only the efficiency of the adsorption process but also the adsorption rate. In the case of using 0.1 g adsorbent, the equilibrium state, which was reached in 30 min, was reached in about 15 min when 0.5 g adsorbent was used. A short time to reach equilibrium in the adsorption process is

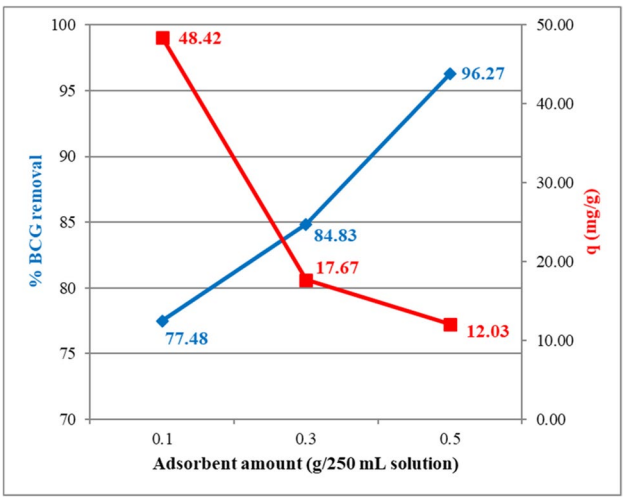

Fig. 6 The % removal efficiency and adsorption capacity values achieved in BCG removal from aqueous solution at different adsorbent amount (C_0 = 25 mg/L; T = 45 °C; pH = 2)

advantageous because it allows for faster adsorption, greater efficiency, better control, and lower costs. Especially, faster adsorption is important in applications where time is a critical factor, such as in catalysis, separation processes, and wastewater treatment. Moreover, a shorter time to reach equilibrium also means that the adsorption process can be more easily controlled. This is because the time it takes for the adsorption process to reach equilibrium can be used to optimize the conditions under which adsorption occurs, such as temperature, pressure, and pH. From an economic point of view, a shorter time to reach equilibrium can also lead to lower costs. This is because the shorter time required for adsorption means that less energy and resources are needed to carry out the process, which can lead to lower operating costs and a lower overall cost of production.

3.1.4 Effect of contact time

Contact time is an important parameter that influences the adsorption process and refers to the duration of time that the adsorbate (the substance being removed) comes into contact with the adsorbent. In general, a longer contact time leads to a higher amount of adsorption, as more time is available for the adsorbate to come into contact with the adsorbent surface. However, beyond a certain point, the rate of adsorption slows down, and the adsorption capacity of the adsorbent reaches a maximum value. Thus, the optimal contact time for an adsorption process is the point at which the maximum adsorption capacity is achieved, and the process is economically feasible. Therefore, the effect of contact time on the adsorption process is an essential parameter that must be carefully considered to achieve maximum adsorption capacity while ensuring an economically viable process. To determine the optimum contact time in the adsorption process for BCG removal from aqueous solutions, the total experiment time was kept as 100 min, and the time to reach equilibrium was determined. Figure 7 shows the change of the adsorption capacity over time at different initial BCG concentrations, and determined the optimum equilibrium time of the adsorption system.

As seen in Fig. 7, at the beginning of the adsorption process, the adsorbent surface was relatively clean and available for adsorption, leading to rapid adsorption of the BCG molecules. During this period, the concentration of the adsorbate in the fluid phase decreased quickly, while the amount of adsorbate on the adsorbent surface increased rapidly. Especially from Fig. 7, it was seen that the adsorption rate was quite high in the first 15 min after the adsorption process started, and the change in the adsorption capacity was also high. As the adsorption process continued, the adsorbent surface became gradually occupied by the BCG molecules, and the available surface area for adsorption decreased. Consequently, the

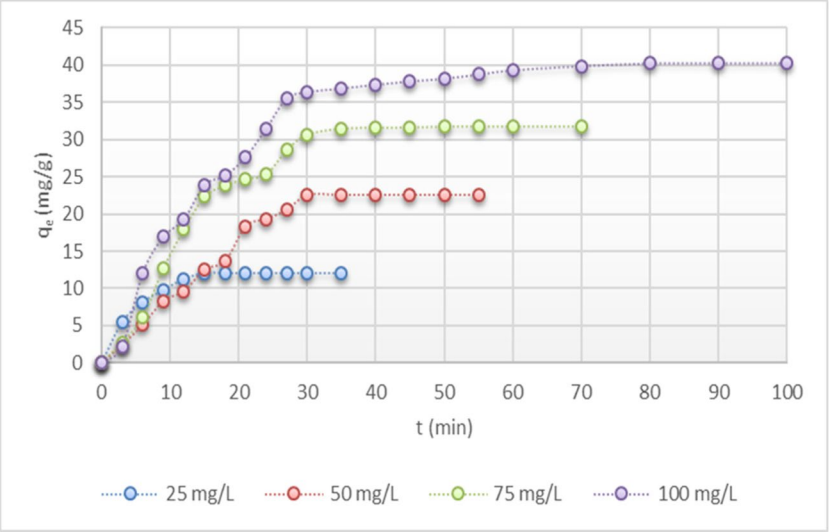

Fig. 7 Variation of adsorption capacity with time at different initial BCG concentration values (pH = 2, adsorbent amount = 0.5 g/250 mL solution; T = 45 °C)

adsorption rate decreased gradually with time. When the adsorbent surface was fully occupied by the adsorbate, the adsorption rate became zero, and the adsorbent has reached saturation. In addition, when equilibrium was reached, the adsorption capacity value remained constant too. Therefore, Fig. 7 showed that there was a significant increase in the time to reach equilibrium with increasing BCG concentration. While the optimum contact time was 15 min at an initial concentration of 25 mg/L, this time increased to 80 min at an initial concentration of 100 mg/L. In other words, although the decreasing initial BCG concentration reduced the adsorption capacity, it shortened the optimum contact time to reach equilibrium. Fast adsorption or short contact time are important parameters in wastewater treatment because they can help to improve the efficiency and effectiveness of the treatment process, reduce operating costs, and improve process control. Especially, when the contact time is short, it is easier to maintain the desired treatment conditions, such as pH and temperature, which can help to optimize the adsorption process. And also, smaller treatment equipment is required to achieve the desired level of treatment, leading to lower capital and operating costs.

The results of the experimental studies showed that KOH-activated pinecone biochar, which is low cost and environmentally friendly, has a very high efficiency in removing BCG dye from aqueous solutions compared to other adsorbents that are expensive and laborious to prepare in the literature. And also, it can be seen that PC-AB has a relatively large adsorption capacity, and short contact time for BCG removal, which is attributed to its surface properties. As a result, this study showed that PC-AB can be considered as a very effective adsorbent for the removal of BCG dye. Table 2 compares the % adsorption efficiency of various adsorbents used for BCG dye removal from aqueous solutions in the literature with the results obtained in this study.

Table 2 Maximum adsorption efficiencies (%) for removal of BCG dye using different adsorbents

Adsorbent	Ambient conditions	Initial concentration (mg/L)	Adsorbent dosage (g/L)	Contact time (min)	Dye removal (%)	Reference
KOH-activated pine cone biochar	45 °C pH = 2	25	2.0	15	96.27	**This study**
H_3PO_4 function. corn cob	50 °C pH = 4	100	2.0	40	99.10	[50]
Chitosan poly(methacrylate) composites	25 °C pH = 2	5	2.0	40	98.50	[51]
Chitin nanofibers	25 °C pH = 6	0.4	1.5	10	92.75	[52]
Poly(2-phenoxy ethyl [bis(2-hydroxy ethyl)amino]acetate)	25 °C pH = 6	100	1.0	90	> 90.00	[53]
ZnO nanorods loaded on activated carbon	25 °C pH = 6	9	0.4	–	99.80	[54]

3.1.5 Adsorption isotherm models

The adsorption isotherm model is a mathematical representation that describes the relationship between the concentration of adsorbate remaining in the solution and the amount of adsorbate adsorbed onto a solid surface at a given temperature. It provides information about the adsorption behavior and helps in understanding the interaction between the adsorbate and adsorbent. The importance of adsorption isotherm models lies in their ability to provide insights into the adsorption process and enable the prediction and optimization of adsorption systems [55]. Especially, adsorption isotherm models enable the comparison of different adsorbents by providing a quantitative measure of their adsorption capacity and affinity. This allows for the evaluation of the performance of different adsorbents and selection of the most appropriate one for a specific application.

In literature, the Langmuir, Freundlich, and Temkin isotherms are three commonly used models to describe the adsorption behavior and characterize the relationship between the equilibrium concentration of adsorbate and the amount of adsorbate adsorbed onto a solid surface. While these isotherms provide valuable insights into adsorption behavior, they are empirical models with their own limitations. The choice of the appropriate isotherm depends on the system being studied and the assumptions that best represent the adsorption process.

Langmuir isotherm model assumes that adsorption occurs at specific sites on the surface of the adsorbent, forming a monolayer of adsorbate. The key assumptions of the Langmuir isotherm are (1) adsorption occurs on a homogeneous surface with a fixed number of identical sites, (2) the adsorption of one molecule does not influence the adsorption of other molecules, and (3) all adsorption sites have the same energy and affinity for the adsorbate. Whereas, the Freundlich isotherm model is an empirical equation that describes heterogeneous adsorption systems where multiple layers of adsorbate can form on the surface. The Temkin isotherm model incorporates the effect of adsorbate-adsorbent interactions on the adsorption process. It assumes that the heat of adsorption decreases linearly with the surface coverage [56]. The linear form of the Langmuir (Eq. 6), Freundlich (Eq. 7), and Temkin (Eq. 8) equations are commonly given by:

$$\frac{C_e}{q_e} = \frac{C_e}{q_{max}} + \left(\frac{1}{q_{max}K_L}\right) \tag{6}$$

$$\ln q_e = \ln K_f + \frac{1}{n}\ln C_e \tag{7}$$

$$q_e = B\ln A + B\ln C_e \tag{8}$$

where C_e is the equilibrium concentration of the adsorbate (mg/L), q_e is the amount of adsorbate adsorbed per unit mass of adsorbent (mg/g), q_{max} is the maximum adsorption capacity (monolayer coverage) of the adsorbent (mg/g), K_L is the constant related to the free energy of adsorption (L/mg), K_f is the Freundlich constant related to the adsorption capacity [mg/g (L/mg)1/n], and n is the Freundlich exponent indicating the adsorption intensity or surface heterogeneity. The value of n determines whether the adsorption is favorable ($n > 1$), linear ($n = 1$), or unfavorable ($n < 1$). A is the equilibrium binding constant (L/g) for Temkin isotherm model, and B is the constant related to the adsorption heat (J/mol) [57, 58].

The fundamental attributes of the Langmuir isotherm can be effectively described using a dimensionless equilibrium parameter known as R_L (Eq. 9). The R_L values serve as indicators for the nature of the isotherm: unfavorable ($R_L > 1$), linear ($R_L = 1$), favorable ($0 < R_L < 1$), or irreversible ($R_L = 0$).

$$R_L = \frac{1}{(1 + K_L C_o)} \tag{9}$$

With the application of the experimental results to the Langmuir, Freundlich, and Temkin isotherm models, linear plots obtained from C_e/q_e versus C_e, $\ln q_e$ versus $\ln C_e$, and q_e versus $\ln C_e$ at each temperature were drawn for adsorption of BCG onto PC-AB. The model parameters calculated from these graphs and the related correlation coefficient (R^2) values are given in Table 3.

In Table 3, it is observed that the correlation coefficients ranked the models in the following descending order: Temkin > Freundlich > Langmuir. Based on the R^2 values, the experimental data is found to be suitable for the Temkin isotherm model. According to this model, it is thought that the heat of adsorption for all BCG molecules exhibits a linear decrease as the adsorbent surface coverage increases. Furthermore, the adsorption process can be characterized by a uniform distribution of binding energies, extending up to the maximum binding energy [59]. According to the this model, the constant related to the adsorption heat was calculated to be 2.80 J/mol at a temperature of 45 °C, which corresponds to the temperature at which the maximum removal efficiency is attained. In addition, adsorption intensity (n) values of the Freundlich isotherm model demonstrated that the BCG adsorption by PC-AB was more favorable at high temperatures. At the same time, the value of n derived from the Freundlich isotherm analysis was consistently found to be greater than 1 across all temperatures examined. Hence, it can be concluded that PC-AB is well-suited for the adsorption of BCG. Based on the obtained 1/n data, which was found to be less than 1, it can be concluded that the adsorption process occurs through chemical adsorption. Based on

Table 3 Langmuir, Freundlich, and Temkin isotherm constants for the adsorption of BCG dye onto PC-AB

Dye	Isotherm model	Parameters	Temperature (°C)		
			25	35	45
$q_{exp.}$ (mg/g)			11.84	11.99	12.03
BCG	Langmuir	q_{max} (mg/g)	8.75	6.73	4.12
		K_L (L/mg)	1.75	0.68	0.25
		R_L	0.02	0.06	0.14
		R^2	0.92	0.90	0.91
	Freundlich	K_f [mg/g (L/mg)$^{1/n}$]	30.85	34.81	15.63
		n	1.57	1.42	3.23
		1/*n*	0.64	0.70	0.31
		R^2	0.96	0.94	0.91
	Temkin	R^2	0.99	0.98	0.99
		A	0.0013	0.0024	0.0064
		B	1.97	2.21	2.80

the Langmuir isotherm model, the dimensionless separation factor (R_L) values, which indicate a favorable adsorption process, ranged from 0.02 to 0.14 [60]. As a result, the isotherm studies conducted to investigate the adsorption mechanism have demonstrated that PC-AB has proven to be effective in removing BCG from aqueous solutions.

3.1.6 Adsorption kinetics and thermodynamic study

Adsorption kinetics refers to the study of the rate at which molecules or ions from a fluid phase (such as a gas or liquid) adhere to the surface of a solid material. In other words, adsorption kinetics helps in comprehending how adsorbent materials interact with adsorbate molecules. This knowledge contributes to a better understanding of surface phenomena and enables the development of more efficient adsorbents. By understanding the kinetics, it can be enhanced the adsorption capacity and efficiency of materials, leading to improved environmental cleanup techniques. In addition, adsorption kinetics provides valuable information about the surface properties of materials. By analyzing the rate of adsorption, it can be determined the surface area, porosity, and accessibility of adsorption sites. This knowledge is crucial for characterizing and comparing different materials, such as porous materials, zeolites, activated carbon, and nanoparticles, for various applications ranging from removal of environmental pollutants to drug delivery systems. As a result, understanding the kinetics allows to optimize the design and operation of adsorption processes, improving their efficiency, selectivity, and capacity. The pseudo-first-order kinetic model, pseudo-second-order kinetic model, and intraparticle diffusion model are mathematical models commonly used to describe the kinetics of adsorption processes. These models are simplified representations of the complex adsorption process and they serve as useful tools for analyzing adsorption kinetics and providing insights into the rate-determining steps and mechanisms involved in the process [61].

3.1.7 Pseudo-first-order kinetic model

The pseudo-first-order kinetic model assumes that the rate of adsorption is directly proportional to the difference between the initial concentration of the adsorbate and the amount adsorbed at any given time. Mathematically, it can be represented as:

$$\ln\left(q_e - q_t\right) = \ln\left(q_e\right) - k_1 t \tag{10}$$

where q_t is the amount of adsorbate adsorbed at time t (mg/g), q_e is the amount of adsorbate adsorbed at equilibrium (mg/g), and k_1 is the pseudo-first-order rate constant (min^{-1}). The model assumes that the adsorption process follows a first-order reaction, similar to chemical reactions, with a linear relationship between the logarithm of the difference in adsorbate concentration and time. However, this model often fails to accurately describe complex adsorption systems.

3.1.8 Pseudo-second-order kinetic model

The pseudo-second-order kinetic model assumes that the rate of adsorption is proportional to the square of the difference between the initial concentration of the adsorbate and the amount adsorbed at any given time. Mathematically, it can be represented as:

$$\frac{t}{q_t} = \frac{1}{k_2 q_e^2} + \frac{t}{q_e} \tag{11}$$

where k_2 is the pseudo-second-order rate constant (g mg^{-1} min^{-1}). The pseudo-second-order model suggests that the adsorption process occurs through chemisorption,

involving strong chemical interactions between the adsorbate and the adsorbent surface. This model often provides a better fit to experimental data and is more applicable to a wide range of adsorption systems.

3.1.9 Intraparticle diffusion kinetic model

The intraparticle diffusion model is used to describe the diffusion of the adsorbate within the porous structure of the adsorbent. It assumes that the rate-limiting step of the adsorption process is the intraparticle diffusion of the adsorbate from the bulk solution to the adsorbent surface. Mathematically, it can be represented as:

$$q_t = k_i.t^{1/2} + C \quad (12)$$

where k_i is the intraparticle diffusion rate constant (mg/g $min^{0.5}$), t is the time (min), and C is a constant representing the thickness of the boundary layer. The intraparticle diffusion model suggests that the adsorption process involves multiple steps, including external mass transfer, boundary layer diffusion, and intraparticle diffusion. The linear portion of the plot of q_t versus $t^{0.5}$ indicates the intraparticle diffusion rate, while deviations from linearity may indicate the involvement of other adsorption mechanisms [62, 63].

In this study, to examine the mechanism of adsorption process, pseudo-first-order, pseudo-second-order, and intraparticle diffusion adsorption models were used to adjust kinetic experimental data. The linear graphs of $\ln(q_e\text{-}q_t)$ versus t, t/q_t versus t, and q_t versus $t^{0.5}$ are drawn. The values of kinetic parameters (the rate constants of the three models with the correlation coefficients and theoretical adsorption capacity values) of linear form of rate equations are presented in Table 4.

In Table 4, it is observed that the correlation coefficients ranked the kinetic models in the following descending order: pseudo-first-order > intraparticle diffusion > pseudo-second-order. Based on the R^2 values, the experimental data is found to be suitable for the pseudo-first-order kinetic model. In addition, $q_{e(exp)}$ (mg/g) values obtained experimentally and $q_{e(cal)}$ (mg/g) values obtained from the pseudo-first-order model equation were very close to each other. According to this model, the adsorption process was predominantly controlled by the concentration of the BCG at the adsorbent surface and that the rate of adsorption decreased as the PC-AB surface becomes more saturated. In other words, the adsorption of the BCG onto the adsorbent surface appeared to be primarily dependent on the concentration of the adsorbate. Therefore, the validity of this model was limited to a specific concentration and time range. It was suitable when the rate of adsorption is relatively constant within this range. This model simplified the complex adsorption process into a more manageable mathematical framework, making it easier to analyze.

It is important to note that while the pseudo-first-order kinetic model can provide a useful approximation of the adsorption process under certain conditions, it may not accurately represent the actual mechanisms at play in all cases. The real adsorption process can be more complex, and deviations from the model may occur under different conditions or with different adsorbents and adsorbates. Researchers often use the pseudo-first-order model as a starting point for understanding adsorption kinetics, but more sophisticated models may be necessary for a more comprehensive and accurate description of the adsorption process in specific systems. One of these models is undoubtedly the intraparticle diffusion model. The intraparticle diffusion model is a commonly used kinetic model in the context of adsorption processes, particularly for describing the mechanism of solute transport within porous adsorbent particles. It provides insights into the rate-limiting step and the overall adsorption process [61]. As can be seen in Table 4, the intraparticle diffusion kinetic model, which has the highest correlation coefficient after the pseudo-first-order kinetic model in BCG adsorption, can be used to explain the transport and adsorption of BCG molecules in porous PC-AB. As can be

Table 4 Rate constants of pseudo-first-order, pseudo-second-order, and intraparticle diffusion kinetic models with correlation coefficients for BCG adsorption onto PC-AB

		C_o (mg/L)			
		25	50	75	100
Kinetic model	**$q_{e\ (exp.)}$ (mg/g)**	12.03	22.53	31.78	40.24
Pseudo-first-order	$q_{e\ (cal.)}$ (mg/g)	10.28	27.50	32.46	40.70
	k_1 (min^{-1})	0.0821	0.0881	0.0982	0.0641
	R^2	0.960	0.933	0.952	0.966
Pseudo-second-order	$q_{e\ (cal.)}$ (mg/g)	21.19	33.10	44.64	51.02
	k_2 (g/mg.min)	0.0079	0.00069	0.00065	0.0010
	R^2	0.817	0.610	0.714	0.828
Intraparticle diffusion	k_i (mg/g.$min^{0.5}$)	1.9754	3.9603	4.4674	4.8161
	C	1.191	2.318	1.437	4.901
	R^2	0.948	0.921	0.906	0.842

seen Fig. 8, adsorption of BCG onto PC-AB encompassed both surface diffusion (movement of solute on the external surface) and pore diffusion (movement within the pores of the adsorbent) by creating two zones. These multiple steps, including external film diffusion and surface adsorption, contributed to the overall BCG adsorption kinetics. The fact that the graph consists of multiple linear sections showing different stages of adsorption has led to a more comprehensive understanding of adsorption processes. At the same time, this model helped in characterizing the rate at which BCG molecules move from the external solution into the interior of PC-AB adsorbent particles. As the initial concentration of BCG molecules increased, rate constant (k_i) were increased and therefore adsorption was faster at higher initial concentrations. As a result, a higher intraparticle diffusion rate constant suggested faster intraparticle mass transfer. In other words, a higher intraparticle diffusion rate constant (k_i) suggested that BCG molecules move relatively quickly within the PC-AB.

Linear and non-linear regression serve as statistical modeling techniques aimed at comprehending and quantifying the interconnection between independent and dependent variables within a dataset. While linear regression assumes a straight-line relationship between the independent and dependent variables, non-linear regression allows for more intricate associations, accommodating various forms like exponential, logarithmic, polynomial, or sigmoidal equations. Non-linear regression proves valuable when the relationship between variables surpasses the simplicity of linear modeling, offering a solution for scenarios where linear equations fail to capture the underlying complexity. Some common types of error functions used in both linear and non-linear regression are mean squared error (MSE), mean absolute error (MAE), root mean squared error (RMSE), sum of squared errors (SSE), Chi-square (χ^2) statistic, and absolute relative error (ARE). The Chi-square statistic is a measure used in hypothesis testing to determine whether there is a significant difference between the expected and observed frequencies in one or more categories. Absolute relative error (ARE) is a metric used to evaluate the accuracy of a model's predictions by measuring the relative difference between the predicted and actual values. Sum of squared errors (SSE) is a common error function used in regression analysis to evaluate the performance of a regression model. SSE quantifies the discrepancy between the observed and predicted values, with smaller values indicating a better fit of the model to the data. Minimizing SSE is often a goal in regression analysis, as it leads to a better fitting model [64].

In this study, statistical modeling was carried out for both linear and non-linear regression using these three important error functions (SSE, ARE, and χ^2), with the help of Eqs. 13–15. The results obtained are given in Tables 5 and 6.

$$\chi^2 = \sum_{i=1}^{n} \frac{(q_{exp.} - q_{pred.})^2}{q_{pred.}} \tag{13}$$

$$\mathrm{SSE} = \sum_{i=1}^{n} (q_{exp.} - q_{pred.})^2 \tag{14}$$

$$\mathrm{ARE} = \frac{1}{n} \sum_{i=1}^{n} \left| \frac{q_{exp.} - q_{pred.}}{q_{exp.}} \right| \tag{15}$$

In the given equations, $q_{exp.}$ represents the experimental value for *i*th adsorbed quantity; $q_{pred.}$ is the predicted value of adsorbed quantity, and *n* is the total number of experiments [65].

The analysis of error functions substantiated the superiority of non-linear regression over linear regression. The non-linear isotherm and kinetic models exhibited lower SSE, ARE, and χ^2 values compared to their linear counterparts. This observation solidified the notion that non-linear equations adeptly capture the intricacies of the adsorption process better than linear models. The diminished χ^2 values in

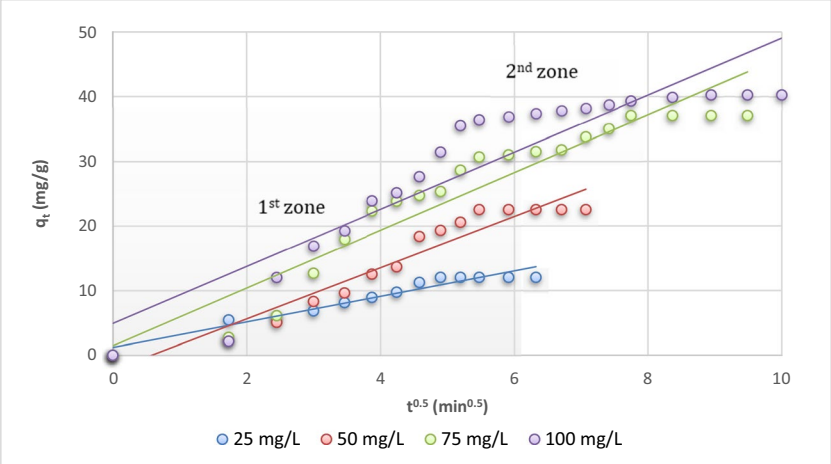

Fig. 8 Intraparticle diffusion kinetic model curves obtained at different initial BCG concentrations

Table 5 Error functions of linear and non-linear isotherm models

Isotherm models	Isotherm errors	Error functions	Temperature (°C)		
			25	35	45
Langmuir	Linear	SSE	1.3206	0.8095	0.8549
		ARE	0.0164	0.0390	0.0512
		χ^2	0.1240	0.0864	0.1120
	Non-linear	SSE	0.1517	1.1014	0.1948
		ARE	0.0111	0.1863	0.0001
		χ^2	0.0165	0.4374	0.0246
Freundlich	Linear	SSE	0.7404	1.4528	1.0266
		ARE	0.0401	0.0675	0.0485
		χ^2	0.0946	0.1857	0.1152
	Non-linear	SSE	0.000549	0.1067	0.000144
		ARE	0.000719	0.0125	0.000527
		χ^2	0.000065	0.0149	0.000018
Temkin	Linear	SSE	0.0502	0.2211	0.5948
		ARE	0.0071	0.0206	0.0368
		χ^2	0.0047	0.0222	0.0699
	Non-linear	SSE	0.000041	0.000395	0.000014
		ARE	0.000163	0.006753	0.000138
		χ^2	0.000005	0.000133	0.000002

Table 6 Error functions of linear and non-linear kinetic models

Kinetic models	Kinetic errors	Error functions	C_o (mg/L)			
			25	50	75	100
Pseudo-first order	Linear	SSE	2.0038	1.2442	1.7551	1.3340
		ARE	0.2175	0.1110	0.0849	0.0335
		χ^2	0.2569	0.5450	0.9042	0.9403
	Non-linear	SSE	0.4176	1.3955	1.6428	1.0181
		ARE	0.0363	0.2741	0.1798	0.1427
		χ^2	0.0489	0.3652	0.3118	0.8218
Pseudo-second order	Linear	SSE	2.6940	1.1501	1.7623	1.3857
		ARE	0.5763	0.1345	0.1786	0.1945
		χ^2	0.3808	0.0495	0.0583	0.0364
	Non-linear	SSE	5.9915	2.0782	0.9985	0.8176
		ARE	0.9843	0.3186	0.2463	0.2190
		χ^2	0.7603	0.4538	0.2665	0.0614
Intraparticle diffusion	Linear	SSE	3.2529	4.0943	1.9522	1.2362
		ARE	0.2190	0.2291	0.0896	0.1081
		χ^2	1.5082	2.7351	0.0564	0.5153
	Non-linear	SSE	0.5085	0.7533	0.5309	1.0189
		ARE	0.0204	0.0490	0.1197	0.1712
		χ^2	0.0508	0.4370	0.8301	0.9143

the non-linear models, contrasted with those of linear models, indicated that linearization skewed the error distribution between experimental and predicted values. Furthermore, these experimental findings underscored that transforming non-linear isotherm equations into linear forms inadvertently alters their error structure and may contravene the assumptions of standard least squares regarding error variance and normality.

Studying adsorption processes from a thermodynamic perspective is crucial for several reasons, as it provides valuable insights into the underlying energetics and feasibility of adsorption phenomena. Therefore, a thermodynamic perspective on adsorption processes provides a comprehensive

framework for assessing the feasibility, efficiency, and environmental impact of adsorption-based technologies. It guides decision-making in various industries, aids in materials selection, and contributes to the development of sustainable and energy-efficient processes. Especially, by examining the changes in thermodynamic quantities such as Gibbs free energy (ΔG°), enthalpy (ΔH°), and entropy (ΔS°), we can determine whether adsorption is spontaneous (favorable) or non-spontaneous (unfavorable). This information is critical for predicting whether a given adsorption process will occur under specific conditions. At the same time, thermodynamic analysis of adsorption processes is fundamental to our understanding of intermolecular interactions, surface phenomena, and phase equilibria. Thermodynamic parameters (ΔH°, ΔS°, and ΔG°) essential for this analysis are presented in Eq. 16–18. These parameters are computed based on the adsorption equilibrium constant values (K_c) obtained at various temperatures.

$$\Delta G = -RT\ln K_c \tag{16}$$

$$\ln K_c = -\frac{\Delta H}{RT} + \frac{\Delta S}{R} \tag{17}$$

$$K_C = \frac{C_{ads}}{C_e} \tag{18}$$

In the given equations, R (with a value of 8.314 J/mol K) represents the universal gas constant, while T (in Kelvin) denotes the absolute temperature of the solution. C_{ads} signifies the concentration of adsorbed BCG dye at equilibrium, and C_e represents the concentration of BCG dye that remains in the solution at equilibrium [66]. To determine the values of ΔH° and ΔS°, one can utilize the slope and intercept from the plot of $\ln K_c$ against 1/T. The calculated thermodynamic parameters are shown in Table 7.

As can be seen from Table 7, the negative Gibbs free energy for the process suggested that adsorption takes place spontaneously. In essence, the feasibility of the adsorption process was confirmed by this negative Gibbs free energy value. Moreover, the positive ΔH° value (1.48 kJ/mol) indicated that adsorption was an endothermic process, while the positive ΔS° value (28.78 J/mol.K) signified an increase in entropy at the solid/solution interface. Notably, the significantly high positive entropy value implied that BCG dye molecules exhibit a strong affinity for the adsorbent used, leading to their enhanced retention at the interface [10].

Table 7 Thermodynamic parameters of BCG dye adsorption onto PC-AB at different temperatures

Dye	T (°C)	ΔH° (kJ/mol)	ΔS° (J/mol K)	ΔG° (kJ/mol)
BCG	25	1.48	28.78	−7.173
	35			−8.120
	45			−8.595

3.2 Surface characteristics of activated PC biochar (before and after BCG adsorption)

Adsorption process can lead to changes in the surface properties of the adsorbent, such as surface charge, functional groups, or surface roughness. Monitoring these changes can provide valuable information about the adsorption mechanism. Changes in surface characteristics can indicate how effectively the adsorbent material removes or interacts with adsorbate molecules. By comparing the surface properties before and after adsorption, we can assess the efficiency of the adsorption process. Especially, in applications like water treatment, wastewater remediation, and gas purification, understanding the changes in surface characteristics is crucial for ensuring the effectiveness of adsorbent materials in removing pollutants or impurities.

In this study, the change in the surface morphology and chemical structure of activated PC biochar after BCG adsorption was determined by SEM and FT-IR analyses. Figure 9 shows the distribution of functional groups on the adsorbent surface before and after the adsorption process. In Fig. 9, the FT-IR spectrum of PC biochar, activated with KOH, reveals distinctive bands at 2127 and 2300 cm^{-1}, which correspond to stretching vibrations of C≡N and C≡C bonds. The functional groups corresponding to these bands are clearly seen in the spectrum after the adsorption process, and their distribution on the adsorbent surface is similar (C≡N and C≡C stretching vibrations are seen at 2324 and 2117 cm^{-1}). Additionally, there are peaks at 3000 cm^{-1}, attributed to stress vibrations of C-H bonds in aliphatic hydrocarbons. When examining the FT-IR spectrum of

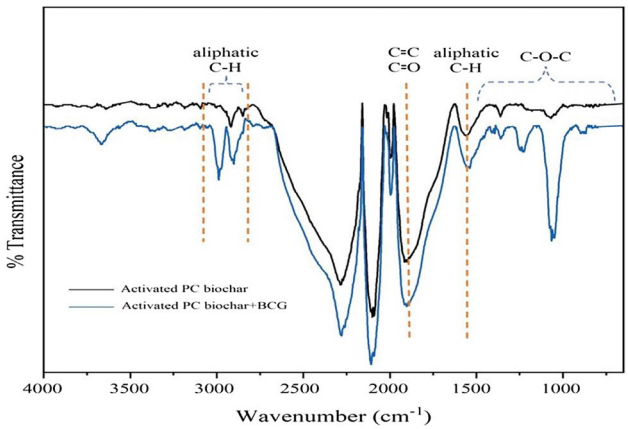

Fig. 9 The FT-IR spectra of the activated PC biochar, both before and after the adsorption of BCG

the activated biochar product after adsorption of BCG, a prominent peak emerges at 3500–3700 cm^{-1}, signifying N–H stretching vibrations originating from amine group compounds. Furthermore, the C-H stretching vibrations from aliphatic hydrocarbons are discernible at 3000 and 2953 cm^{-1}. Notably, these peaks appear sharper and more pronounced following the adsorption of BCG. Consistently, across all spectra, vibrations associated with C-O, C-N, and C–C stress are evident in the range of approximately 1000–1500 cm^{-1}. These vibrations exhibit enhanced intensity in the spectrum recorded after the adsorption of BCG. This heightened intensity can be attributed to the presence of oxygen-containing groups within the chemical structure of the BCG dye [67]. Specifically, it is plausible that functional groups such as C≡N, C-O, and C-N groups, which are present on the biochar surface, played a crucial role in binding the dyes to the biochar surface [67–71].

SEM analysis is a versatile and powerful tool for investigating the micro- and nano-scale properties of materials. This technique offers high-resolution imaging capabilities, enabling the observation of fine details and small structures that may not be visible with other optical microscopy techniques. It can magnify samples at much higher levels, typically up to several hundred thousand times, providing a deeper insight into the sample's structure. In this study, SEM analysis allowed to visualize and analyze the surface morphology and topography of PC-AB at a micro- or nanoscale level. This is crucial for understanding the physical characteristics, textures, and structural features of the adsorbent. In Fig. 10, the highly porous surface morphology of PC-AB, whose surface area is increased through chemical activation, is clearly seen. This porosity enabled the BCG dye molecules to be loaded into the adsorbent with high efficiency. When the characteristic patterns of PC-AB before and after adsorption are examined, it is clearly seen that the BCG dye molecules adhering to the active sites on the adsorbent surface and inside the pores cause a change in the surface morphological structure of the adsorbent and lead to the emergence of a smoother and more regular pattern compared to the initial state. FT-IR analysis also strongly supports this conclusion.

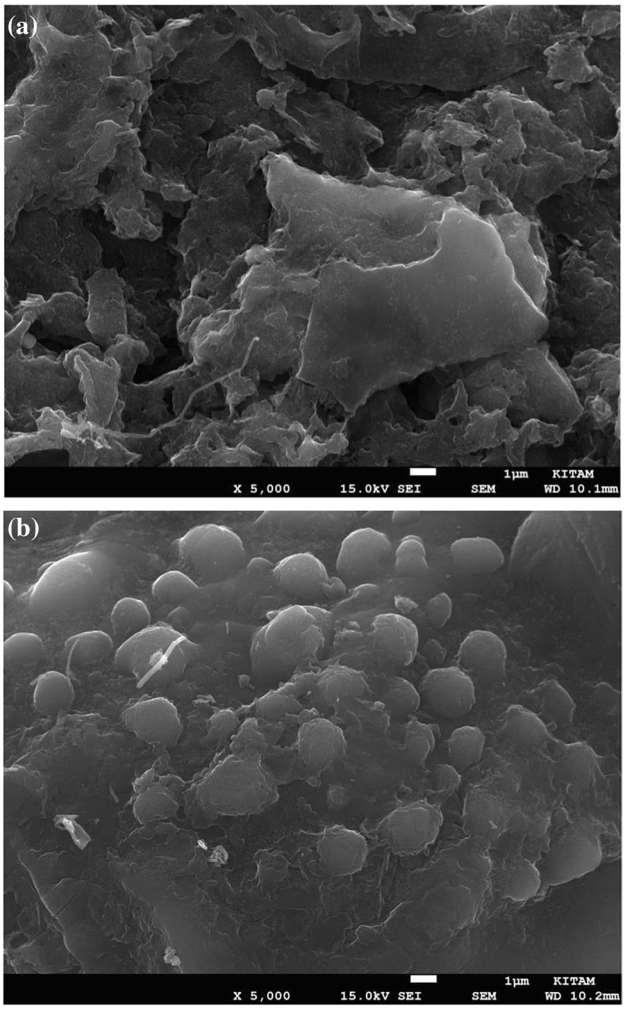

Fig. 10 SEM images of the activated PC biochar **a** before BCG adsorption, **b** after BCG adsorption

3.2.1 ANN modeling

In this study, artificial neural networks (ANN) were used to model BCG removal with the help of activated biochar obtained from PC. Temperature, pH, adsorbent dosage, initial dye concentration, and contact time were selected as input parameters. The Levenberg Marquardt back propagation algorithm was used to predict BCG removal from aqueous solution. This algorithm, which is included in MATLAB was chosen since if often has higher rates of convergence than the other algorithm provided in the toolbox. ANN modeling was performed using Matlab. The data was randomly divided into 3 sets; 70% for training the network, 15% for validation, and 15% for testing. In which 125 samples for training, 27 samples for validation, and 27 samples were used for testing. Root mean square error (RMSE), mean absolute error (MAE), mean bias error (MBE), and determination of coefficient (R^2) are statistical parameters used to evaluate models [25, 26]. The performance of the selected model was evaluated with different statistical parameters such as R^2, MAE, RMSE, and MBE. Minimum MAE, RMSE, and MBE were taken to find the best network topology.

The performance results of the different network structures for experimental data are presented in Table 8. In this study, 42 ANN models with different network structures were developed and explored the applicability. Figure 1 illustrates the architecture of the chosen ANN26 model in the network construction. The training, validation, and test

Table 8 The comparisons performance of different ANN network structure

No	Network ınputs	Network structure	Transfer functions		RMSE	MBE	MAE	R^2
			Hidden layer	Output layer				
ANN1	Temperature, pH, adsorbent dosage, initial dye concentration, contact time	1–1	Tangent	Purelin	10.339	8.462	0.407	0.924
ANN2		3–1	Tangent	Purelin	9.715	7.624	−1.724	0.950
ANN3		5–1	Tangent	Purelin	2.224	1.392	−0.083	0.999
ANN4		7–1	Tangent	Purelin	2.001	1.096	0.206	0.999
ANN5		10–1	Tangent	Purelin	1.928	1.157	−0.026	0.999
ANN6		15–1	Tangent	Purelin	1.545	0.838	0.023	0.999
ANN7		3–3-1	Tangent	Purelin	9.759	7.458	0.159	0.920
ANN8		3–5-1	Tangent	Purelin	8.035	6.061	1.271	0.971
ANN9		3–7-1	Tangent	Purelin	5.152	3.960	−0.298	0.966
ANN10		3–10-1	Tangent	Purelin	2.051	1.400	0.184	0.999
ANN11		3–15-1	Tangent	Purelin	3.740	2.537	0.094	0.993
ANN12		3–20-1	Tangent	Purelin	3.032	1.865	−0.258	0.999
ANN13		3–25-1	Tangent	Purelin	1.945	1.253	0.208	0.999
ANN14		3–30-1	Tangent	Purelin	2.659	1.687	−0.100	0.990
ANN15		5–5-1	Tangent	Purelin	3.113	2.198	−0.043	0.996
ANN16		5–7-1	Tangent	Purelin	2.055	1.235	−0.017	0.999
ANN17		5–10-1	Tangent	Purelin	2.333	1.187	−0.164	0.999
ANN18		5–15-1	Tangent	Purelin	1.516	0.760	0.019	0.999
ANN19		5–20-1	Tangent	Purelin	1.624	1.036	−0.144	0.997
ANN20		5–25-1	Tangent	Purelin	1.756	0.964	0.026	0.998
ANN21		5–30-1	Tangent	Purelin	1.277	0.512	−0.019	0.999
ANN22		5–40-1	Tangent	Purelin	1.035	0.566	−0.047	0.999
ANN23		5–50-1	Tangent	Purelin	1.340	0.584	−0.045	0.998
ANN24		7–7-1	Tangent	Purelin	2.155	1.356	−0.278	0.999
ANN25		7–10-1	Tangent	Purelin	1.466	0.787	−0.084	0.999
ANN26		**7–15-1**	**Tangent**	**Purelin**	**0.947**	**0.578**	**0.036**	**0.999**
ANN27		7–20-1	Tangent	Purelin	1.690	0.928	0.063	0.998
ANN28		7–25-1	Tangent	Purelin	1.615	0.854	−0.036	0.999
ANN29		7–30-1	Tangent	Purelin	1.115	0.589	−0.056	0.999
ANN30		10–10-1	Tangent	Purelin	1.729	0.790	−0.010	0.999
ANN31		10–15-1	Tangent	Purelin	1.559	0.747	−0.047	0.999
ANN32		10–20-1	Tangent	Purelin	1.521	0.891	0.177	0.999
ANN33		10–25-1	Tangent	Purelin	1.591	0.798	−0.014	0.999
ANN34		10–30-1	Tangent	Purelin	1.596	0.739	−0.047	0.999
ANN35		15–15-1	Tangent	Purelin	1.554	0.832	0.115	0.999
ANN36		15–20-1	Tangent	Purelin	3.219	1.999	−0.506	0.999
ANN37		15–25-1	Tangent	Purelin	2.031	1.275	−0.019	0.999
ANN38		15–30-1	Tangent	Purelin	1.255	0.734	−0.243	0.999
ANN39		20–20-1	Tangent	Purelin	4.448	2.769	0.074	0.991
ANN40		20–25-1	Tangent	Purelin	2.213	1.177	−0.142	0.999
ANN41		20–30-1	Tangent	Purelin	2.082	0.993	0.147	0.999
ANN42		20–40-1	Tangent	Purelin	2.166	1.116	0.406	0.999

performance of the ANN26 model is given in Fig. 11. Then, the performance of the measured model was evaluated by different statistical parameters such as R^2, RMSE, MBE, and MAE. Table 9 presents the values of these parameters. In general, only one of the 42 models tested had an RMSE value of less than 1.0. As the 7–15-1 model, ANN26 had a lower RMSE (0.947), lower MBE (0.578), and lower MAE (0.036) compared to other models. Low error values (RMSE, MBE, and MAE) and high correlation coefficient (R^2) showed that the ANN26 model was the best among

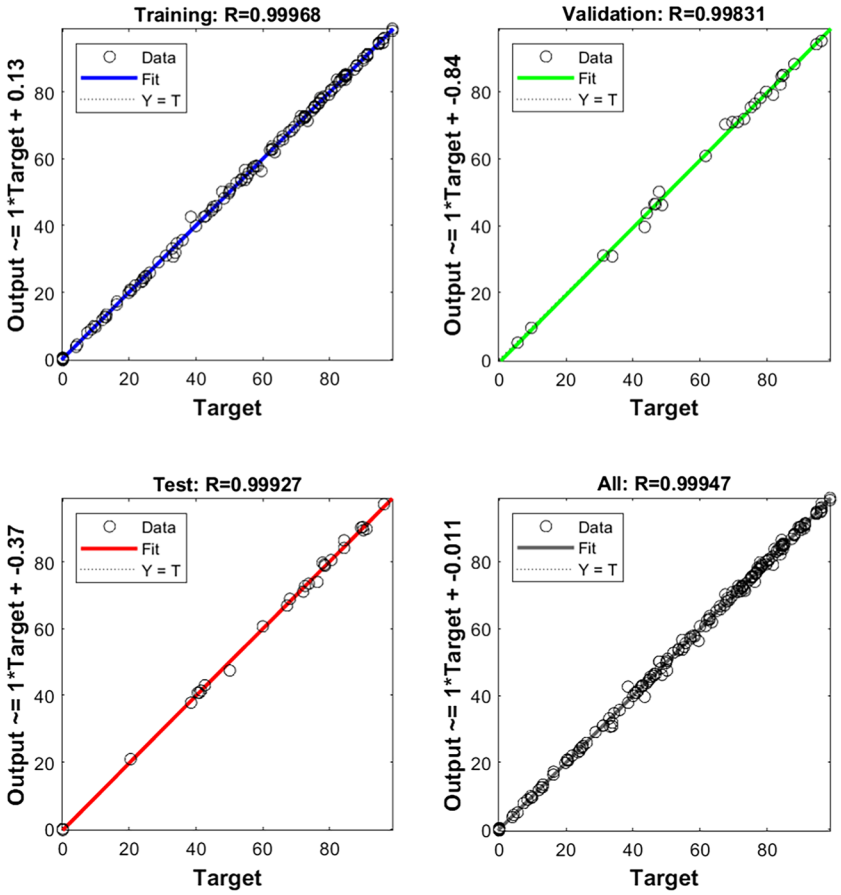

Fig. 11 Training, validation and test performance of ANN26 model

Table 9 Statistical parameters of the ANN26 model

No	Network structure	Statistical parameters				
		Set	RMSE	MBE	MAE	R^2
ANN26	7–15-1	Training	0.969	0.595	0.015	0.999
		Validation	0.891	0.571	0.283	0.997
		Test	0.966	0.560	−0.075	0.999
		All	0.947	0.578	0.036	0.999

many models and the results are presented in Table 9. The model developed (ANN26) was successful in predicting the BCG adsorption capacity of activated PC biochar, as shown in Fig. 11. The output of the model was strongly compatible with the observed values.

As a result, artificial neural network is a model used to examine the effects of variable parameters on output. Correlation graphs for the estimation of % removal efficiency using single or multiple components of adsorption analyzes are presented in Fig. 12. Temperature, pH, adsorbent dosage, initial dye concentration, and contact time were chosen as input parameters in adsorption studies. These parameters are represented by the symbols T, pH, m, C_o, and t, respectively. As shown in Fig. 12, the effects of the adsorbent dosage, pH, and temperature variables on output alone were very small, since the correlation values were low. Although the initial dye concentration had an effect on the output, it was insufficient on its own. Although it was seen that the correlation increased with the addition of adsorbent dosage and contact time variables to this variable, it was not satisfactory for the % removal efficiency estimations. Therefore, the temperature, pH, adsorbent dosage, initial dye concentration, and contact time variables were all used to accurately estimate the % removal efficiency, and the highest correlation was obtained using these variables.

3.3 Regeneration and reusability of activated PC biochar

Regenerating adsorbents is crucial for economic, environmental, and operational reasons, ensuring the efficient and

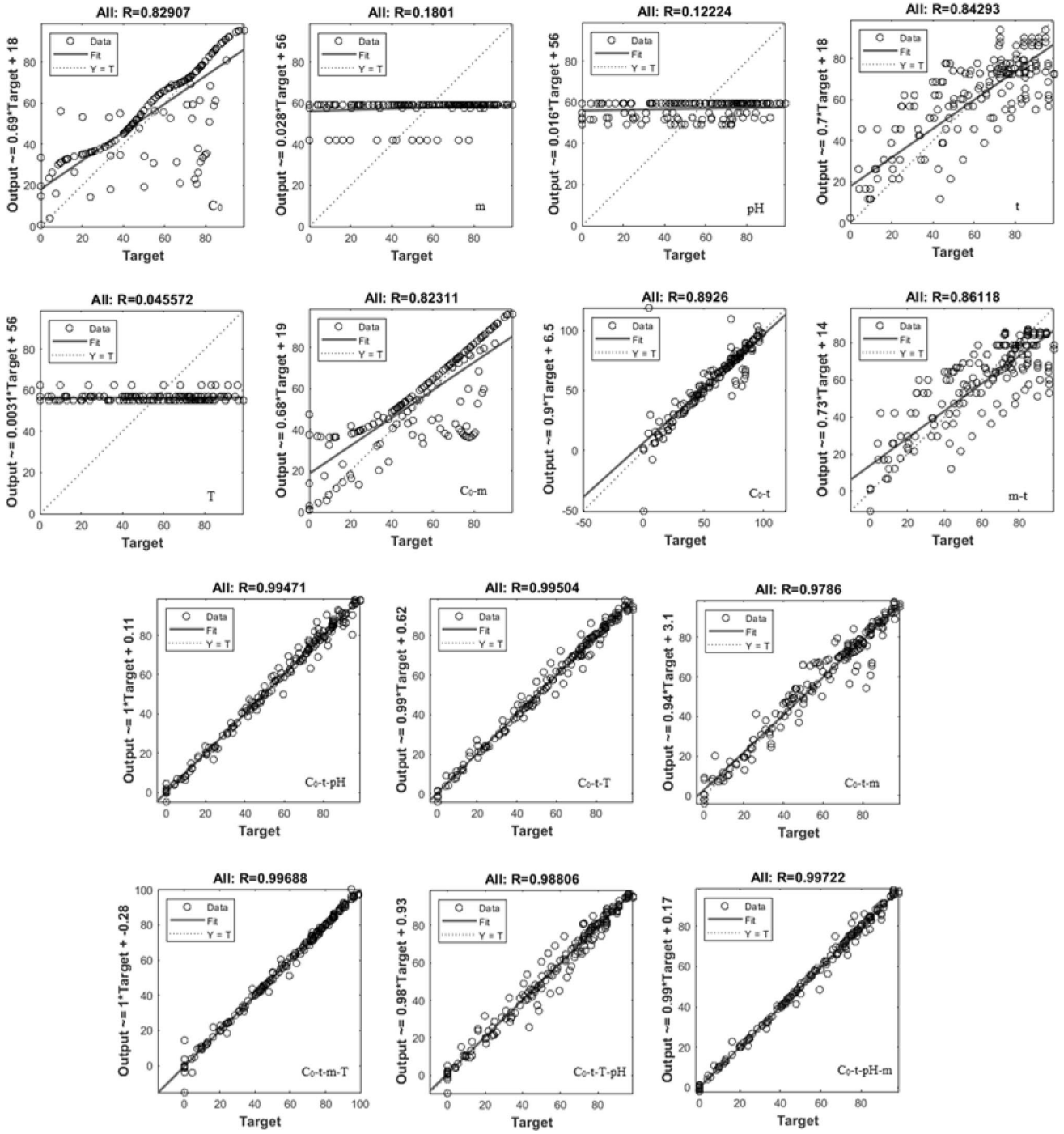

Fig. 12 Relationships between % removal efficiency and input parameters

sustainable use of these materials in various applications, such as water purification, air quality control, and chemical processing. Especially, the regeneration of adsorbents for subsequent reuse stands out as a paramount factor in assessing performance. In this study, after regeneration process, the adsorption performance of PC-AB remained consistently high, exceeding 95% throughout four cycles of recycling tests (96.1% for $n=1$, 96.0% for $n=2$, 95.7% for $n=3$, and 95.0% for $n=4$). These results from the recovery tests highlight the suitability of PC-AB as a recyclable adsorbent for the efficient removal of BCG from solutions. Nevertheless, by the 5th cycle, the removal efficiency of BCG on regenerated activated PC biochar had notably decreased by approximately 35%. This considerable decline in adsorption

capacity is primarily attributed to an incomplete desorption process. Consequently, the recycling studies showed that the adsorption efficiency of PC-AB was high even after four adsorption and desorption cycles [72].

4 Conclusions

In this study, lignocellulosic PC biomass, which is one of the important forest wastes, was used as raw material and activated PC biochar was obtained by performing pyrolysis and chemical activation processes together. Biochar containing 89.9% carbon by weight was characterized and used as an adsorbent in the removal of BCG dye from aqueous media. KOH used in the chemical activation process prevented the formation of tar and volatile substances, thus increasing the biochar yield. In addition, it also caused a significant increase in surface area. This alkaline modification process applied in the production of activated PC biochar, whose BET surface area and pore volume values are 1714.5 m^2/g and 0.684 cm^3/g, respectively, caused a decrease in the oxygen-containing functional groups and an increase in the hydroxyl functional group (OH^-) in the structure of the biochar. Thus, it increased the adsorption efficiency of non-polar pollutants, especially anionic dye such as BCG. By determining the effects of various process variables on the adsorption process, optimum adsorption conditions were determined. Accordingly, the optimum adsorption conditions for BCG removal from aqueous solutions were determined as pH = 2.0, T = 45 °C, C_o = 25 mg/L and adsorbent dosage 2 g/L. Under these conditions, the maximum BCG removal efficiency achieved in 15 min of contact time was calculated as 96.27%. Experimental results concluded that this activated biochar product is a superior adsorbent for BCG removal. In the continuation of the study, the kinetic and thermodynamic parameters of the adsorption process were determined. It was determined that the experimental results were more compatible with the Temkin isotherm model and the pseudo-first-order kinetic model due to the highest correlation coefficient. In BCG adsorption onto activated PC biochar, the Gibbs free energy (ΔG°), enthalpy (ΔH°), and entropy (ΔS°) change were − 8.595 kJ/mol (at 45 °C), 1.48 kJ/mol and 28.78 J/mol K, respectively. These results demonstrated the spontaneous, endothermic, and increasing randomness nature of BCG adsorption. The regenerated activated PC biochar showed good performance (95.0%) for the removal of BCG dye molecules, even, after 4th regeneration. In the final stage of the study, the results obtained from the effects of temperature, pH, adsorbent dosage, initial dye concentration, and contact time were established into an artificial neural network (ANN) as input parameters, and the prediction of adsorption capacity of the activated biochar was modeled. To predict the BCG adsorption capacity, many different ANN models have been developed. The optimal ANN model gave mean absolute error (MAE), mean bias error (MBE), root mean square error (RMSE), and R^2 values of 0.036, 0.578, 0.947, and 0.999, respectively, when compared with the experimental data. The results obtained showed that ANN can be used to effectively model the BCG adsorption process.

Consequently, studies have revealed that employing PCs as a biomass source for biochar production represents a sustainable and economically efficient method for generating biochar. Biochar, with its diverse applications in agriculture, forestry, and environmental remediation emerges as a versatile product. These research outcomes have not only offered an environmentally conscious solution but have also presented an economical adsorbent for effectively eliminating BCG dye from aqueous solutions.

Acknowledgements The authors would like to thank Hitit University for its support and also would like to thank to Assoc. Prof. Dr. Yunus Onal for his support in the preparation of activated biochar product.

Author contribution Conceptualization, methodology, investigation, writing-original draft preparation, review and editing: N. Kaya; artificial intelligence application: Z. Yıldız Uzun. All authors read and approved the final manuscript.

Funding Open access funding provided by the Scientific and Technological Research Council of Türkiye (TÜBİTAK).

Data availability All data generated or analyzed during this study are included in this published article.

Declarations

Ethics approval Not applicable.

Consent to participate Not applicable.

Competing interests The authors decalre no competing interests.

References

1. Halder JN, Islam MN (2015) Water pollution and its impact on the human health. J Environ Hum 2(1):2373–8332
2. Abdi J, Vossoughi M, Mahmoodi NM, Alemzadeh I (2017) Synthesis of metal-organic framework hybrid nanocomposites based on GO and CNT with high adsorption capacity for dye removal. Chem Eng J 326:1145–1158
3. Radoor S, Karayil J, Jayakumar A, Raj KD, Kim JT, Siengchin S, Lee J (2024) Recent advances in cellulose- and alginate-based hydrogels for water and wastewater treatment: a review. Carbohyd Polym 323:121339
4. Bakar NA, Othman N, Yunus ZM, Altowayti WAH, Tahir M, Fitriani N, Mohd-Salleh SNA (2021) An insight review of lignocellulosic materials as activated carbon precersor for textile wastewater treatment. Environ Technol Innov 22:101445
5. Radoor S, Karayil J, Jayakumar A et al (2023) Polyvinyl alcohol/guar gum-based bio-adsorbent for the removal of cationic and anionic dyes from aqueous solution. Polym Bull 80:10165–10191
6. Arıkan EB, Isik Z, Bouras HD, Dizge N (2019) Investigation of immobilized filamentous fungi for treatment of real textile industry wastewater using up flow packed bed bioreactor. Bioresour Technol Rep 7:100197
7. Kishor R, Purchase D, Saratale GD, Saratale RG, Ferreira LFR, Bilal M, Chandra R, Bharagava RN (2021) Ecotoxicological and health concerns of persistent coloring pollutants of textile industry wastewater and treatment approaches for environmental safety. J Environ Chem Eng 9(2):105012
8. Funnekotter B, Mancera RL, Bunn E (2023) A simple but effective combination of pH indicators for plant tissue culture. Plants 12(4):740
9. Trivedi VD, Saxena I, Siddiqui MU, Qasim MA (1997) Interaction of bromocresol green with different serum albumins studied by fluorescence quenching. Biochem Mol Biol Int 43(1):1–8
10. Murmu BM, Behera SS, Das S, Mohapatra RK, Bindhani BK, Parhi PK (2018) Extensive investigation on the study for the adsorption of bromocresol green (BCG) dye using activated Phragmites karka. Indian J Chem Technol 25:409–420
11. Gupta VK, Suhas (2009) Application of low-cost adsorbents for dye removal-A review. J Environ Manage 90(8):2313–2342
12. Harshananda TN, Ayisha TM, Janani Priyanka PR, Dildar Mather KN, Vijayakumar R (2020) Removal of colour from textile effluent by adsorption using banana stem and coffee husk: a review. IOSR J Mech Civ Eng 17(4):32–41
13. Rathi BS, Kumar PS (2021) Application of adsorption process for effective removal of emerging contaminants from water and wastewater. Environ Pollut 280:116995
14. Crini G (2006) Non-conventional low-cost adsorbents for dye removal: a review. Biores Technol 97(9):1061–1085
15. Leimkuehler EP (2010) Production, characterization, and applications of activated carbon. Master of Science Thesis, Faculty of the Graduate School University of Missouri, Columbia, Dr. Galen J. Suppes Thesis Supervisor. https://doi.org/10.32469/10355/8078
16. Waqas M, Asam Z, Rehan M, Anwar MN, Khattak RA, Ismail IMI, Tabatabaei M, Nizami AS (2020) Development of biomass-derived biochar for agronomic and environmental remediation applications. Biomass Convers Biorefin 11:339–361
17. Bushra B, Remya N (2020) Biochar from pyrolysis of rice husk biomass-characteristics modification and enviromental application. Biomass Convers Biorefin. https://doi.org/10.1007/s13399-020-01092-3
18. Biswas S, Siddiqi H, Meikap BC, Sen TK, Khiadani M (2020) Preparation and characterization of raw and inorganic acid-activated pine cone biochar and its application in the removal of aqueous-phase Pb^{2+} metal ions by adsorption. Water Air Soil Pollut 231:3
19. Güleç A, Tolunay A (2021) The contribution of umbrella pinus forests (pinus pinea l.) to village legal entities and local economy: the case of gediz basin. Int Sci Vocat Stud J 5(1):19–33
20. Meneses DB, Oca-Vásquez GM, Vega-Baudrit JR, Rojas-Álvarez M, Corrales-Castillo J, Murillo-Araya LC (2022) Pretreatment methods of lignocellulosic wastes into value-added products: recent advances and possibilities. Biomass Convers Biorefin 12:547–564
21. Mohan D, Pittman CU Jr, Steele PH (2006) Pyrolysis of wood/biomass for bio-oil: a critical review. Energy Fuels 20:848–889
22. Kwiatkowski M, Broniek E (2017) An analysis of the porous structure of activated carbons obtained from hazelnut shells by various physical and chemical methods of activation. Colloids Surf, A 529:443–453
23. Kwikima MM, Chebude Y, Meshesha BT (2023) Cadmium removal from aqueous solution by blended bamboo sawdust/rice-husk biochar; optimization of influencing parameters. Int J Phytorem 25(11):1397–1412
24. Pauletto PS, Lütke SF, Dotto GL, Salau NPG (2021) Modeling pseudo-second-order kinetics of orange peel-paracetamol adsorption process using artificial neural network. Chem Eng J 412:127527
25. Afolabi IC, Popoola SI, Bello OS (2020) Machine learning approach for prediction of paracetamol adsorption efficiency on chemically modified orange peel. Spectrochim Acta Part A Mol Biomol Spectrosc 243:118769
26. Praveen S, Jegan J, Pushpa TB, Gokulan R (2021) Artificial neural network modelling for biodecolorization of Basic Violet 03 from aqueous solution by biochar derived from agro-bio waste of groundnut hull: Kinetics and thermodynamics. Chemosphere 276:130191
27. Prasad R, Yadav KD (2020) Use of response surface methodology and artificial neural network approach for methylene blue removal by adsorption onto water hyacinth. Water Conserv Manag 4(2):83–89
28. Kaya N, Yıldız UZ, Altuncan C et al (2022) Adsorption of Congo red from aqueous solution onto KOH-activated biochar produced via pyrolysis of pine cone and modeling of the process using artificial neural network. Biomass Conv Bioref 12:5293–5315
29. Radoor S, Karayil J, Parameswaranpillai J et al (2020) Removal of anionic dye Congo red from aqueous environment using polyvinyl alcohol/sodium alginate/ZSM-5 zeolite membrane. Sci Rep 10:15452
30. Wong YJ, Arumugasamy SK, Chung CH, Selvarajoo A, Sethu V (2020) Comparative study of artificial neural network (ANN), adaptive neuro-fuzzy inference system (ANFIS) and multiple linear regression (MLR) for modeling of Cu (II) adsorption from aqueous solution using bio-char derived from rambutan (Nephelium lappaceum) peel. Environ Monit Assess 192(7):439
31. Bi H, Wang C, Jiang X, Jiang C, Bao L, Lin Q (2020) Prediction of mass loss for sewage sludge-peanut shell blends in thermogravimetric experiments using artificial neural networks. Energy Sources A: Recovery Util Environ Eff. https://doi.org/10.1080/15567036.2020.1841338
32 Al-Yaari M, Dubdub I (2020) Application of artificial neural networks to predict the catalytic pyrolysis of HDPE using non-isothermal TGA data. Polymers 12(8):1813
33. Khan EA, Shahjahan KTA (2018) Adsorption of methyl red on activated carbon derived from custard apple (annona squamosa) fruit shell: equilibrium isotherm and kinetic studies. J Mol Liq 249:1195–1211
34. Boutaieb M, Guiza M, Román SS et al (2020) Pine cone pyrolysis: optimization of temperature for energy recovery. Environ Prog Sustain Energy 39(1):13272
35 Boutaieb M, Guiza M, Román S, Nogales S, Ledesma B, Ouederni A (2020) Pine cone pyrolysis: optimization of temperature for energy recovery. Environ Prog Sustain Energy 39:e13272

36. Kaya N, Yıldız UZ (2021) Investigation of effectiveness of pine cone biochar activated with KOH for methyl orange adsorption and CO_2 capture. Biomass Conv Bioref 11:1067–1083
37. Kaya N, Yıldız UZ (2020) Investigation of effectiveness of pyrolysis products on removal of alizarin yellow GG from aqueous solution: a comparative study with commercial activated carbon. Water Sci Technol 81(6):1191–1208
38. Sabzehmeidani MM, Mahnaee S, Ghaedi M, Heidari H, Roy VAL (2021) Carbon based materials: a review of adsorbents for inorganic and organic compounds. Mater Adv 2:598–627
39. Küçükgül EY (2004) Productıon of the commerical activated carbon and determination of the properties. Dokuz Eylul Univ Fac Eng J Sci Eng 6(3):41–56
40. Giannakoudakis DA, Kyzas GZ, Avranas A, Lazaridis NK (2016) Multi-parametric adsorption effects of the reactive dye removal with commercial activated carbons. J Mol Liq 213:381–389
41. Uzunkavak O, Ozdemir G (2019) Removal of lead and cadmium ions from aqueous solutions by olive pomace as a low-cost biosorbent. JOTCSB 2(2):121–132
42. Chham A, Khouya E, Oumam M, Abourriche A, Gmouh S, Larzek M, Mansouri S, Elhammoudi N, Hanafi N, Hannache H (2018) The Use of insoluble matter of moroccan oil shale for removal of dyes from aqueous solution. Chem Int 4(1):67–76
43. Taher T, Putra R, Palapa NR, Lesbani A (2021) Preparation of magnetite-nanoparticle-decorated nife layered double hydroxide and its adsorption performance for congo red dye removal. Chem Phys Lett 777:138712
44. Kecili R., Hussain C.M., Chapter 4 - Mechanism of adsorption on nanomaterials, Editor(s): Chaudhery Mustansar Hussain, Nanomaterials in Chromatography, Elsevier, 2018, 89–115, https://doi.org/10.1016/B978-0-12-812792-6.00004-2.
45. Radoor S, Jayakumar A, Karayil J, Kim JT, Siengchin S (2023) Biodegradable polymeric green adsorbent for the highly efficient removal of crystal violet dye from aqueous solution. Chem Eng Res Des 199:473–485
46. Ileri B (2019) Removal of methyl red dye by adsorption process using modified fly ash with ultrasound process. Dokuz Eylul Univ Fac Eng J Sci Eng 21(61):25–40
47. Rajoriya S, Saharan VK, Pundir AS, Nigam M, Roy K (2021) Adsorption of methyl red dye from aqueous solution onto eggshell waste material: Kinetics, isotherms and thermodynamic studies. Curr Res Green Sustain Chem 4:100180
48. Sabarish R, Unnikrishnan G (2018) Polyvinyl alcohol/carboxymethyl cellulose/ZSM-5 zeolite biocomposite membranes for dye adsorption applications. Carbohyd Polym 199:129–140
49. Okeola FO, Odebunmi EO, Adebayo GB, Ameen OM (2012) Adsorbents from jatropha curcas shells production, utilisation equilibrium, kinetics and thermodynamic studies of their adsorption: a review. Int J Phytofuels Other Allied Sci 1(1):142–150
50. Onu CE, Ohale PE, Ekwueme BN, Obiora-Okafo IA, Okey-Onyesolu CF, Onu CP, Ezema CA, Onu OO (2022) Modeling, optimization, and adsorptive studies of bromocresol green dye removal using acid functionalized corn cob. Clean Chem Eng 4:100067
51. Liu D, Yuan J, Li J, Zhang G (2019) Preparation of chitosan poly(methacrylate) composites for adsorption of bromocresol green. ACS Omega 4:12680–12686
52. Salmalian E, Rezaei H, Shahbazi A (2019) Removal of bromocresol green from aqueous solutions using chitin nanofibers. Environ Resour Res 7(2):79–86
53. Torğut G, Demirelli K (2018) Comparative adsorption of different dyes from aqueous solutions onto polymer prepared by ROP: Kinetic, equilibrium and thermodynamic studies. Arab J Sci Eng 43:3503–3514
54. Ansari F, Ghaedi M, Taghdiri M, Asfaram A (2016) Application of ZnO nanorods loaded on activated carbon for ultrasonic assisted dyes removal: Experimental design and derivative spectrophotometry method. Ultrason Sonochem 33:197–209
55. Günay A, Dikmen S, Ersoy B, Evcin A (2014) Adsorption of basic Blue-16 dye onto clay. Eur J Sci Technol 1(2):29–38
56. Dada AO, Olalekan AP, Olatunya AM, Dada O (2012) Langmuir, Freundlich, Temkin and Dubinin-Radushkevich isotherms studies of equilibrium sorption of Zn^{2+} onto phosphoric acid modified rice husk. IOSR J Appl Chem 3(1):38–45
57. Njewa JB, Shikuku VO (2023) Recent advances and issues in the application of activated carbon for water treatment in Africa: a systematic review (2007–2022). Appl Surf Sci Adv 18:100501
58. Radoor S, Karayil J, Jayakumar A et al (2022) Ecofriendly and low-cost bio adsorbent for efficient removal of methylene blue from aqueous solution. Sci Rep 12:20580
59. Piccin JS, Dotto GL, Pinto LAA (2011) Adsorption isotherms and thermochemical data of FD&C RED N° 40 binding by chitosan. Braz J Chem Eng 28(2):295–304
60. Demir F, Lacin O, Bastaban B (2019) Determined of equilibrium adsorption isotherm model pertechnetate oxoanion onto activated carbon. Sinop Uni J Nat Sci 4(1):37–46
61. Mohammadi A, Karimi AA (2017) Methylene blue removal using surface-modified TiO_2 nanoparticles: a comparative study on adsorption and photocatalytic degradation. J Water Environ Nanotechnol 2(2):118–128
62. Dogan M, Abak H, Alkan M (2009) Adsorption of methylene blue onto hazelnut shell: kinetic, mechanism and activation parameters. J Hazard Mater 164:172–181
63. MB Jacques NP Guy ML Jules et al 2023 Removal of crystal violet by TiO2 loaded alkali-activated carbon hybrid material from Raphia farinifera fruit kernels: surface chemistry, parameters and mechanisms Bioref Biomass Conv https://doi.org/10.1007/s13399-023-04988-y
64. Ngakou CS, Anagho GS, Ngomo HM (2019) Non-linear regression analysis for the adsorption kinetics and equilibrium isotherm of phenacetin onto activated carbons. Curr Appl Sci Technol 36(4):1–18
65. Revellame ED, Fortela DL, Sharp W, Hernandez R, Zappi ME (2020) Adsorption kinetic modeling using pseudo-first order and pseudo-second order rate laws: a review. Clean Eng Technol 1:100032
66. Erdem F, Tosun A, Ergun M (2016) Biosorption of Remazol Yellow (RR) by Saccharomyces cerevisiae in a batch system. J Fac Eng Archit Gazi Univ 31(4):971–978
67. Phuong DTM, Loca NX, Miyanishi T (2019) Efficiency of dye adsorption by biochars produced from residues of two rice varieties, Japanese Koshihikari and Vietnamese IR50404. Desalin Water Treat 165:333–351
68. Ceylan S, Goldfarb JL (2015) Green tide to green fuels: TG–FTIR analysis and kinetic study of Ulva prolifera pyrolysis. Energy Convers Manage 101:263–270
69. Liu S, Chen X, Liu A, Wang L, Yu G (2015) Co-pyrolysis characteristic of biomass and bituminous coal. Biores Technol 179:414–420
70. Niu Z, Liu G, Yin H, Wu D, Zhou C (2016) Investigation of mechanism and kinetics of non-isothermal low temperature pyrolysis of perhydrous bituminous coal by in-situ FTIR. Fuel 172:1–10
71. Odeh AO (2015) Oualitative and quantitative ATR-FTIR analysis and its application to coal char of different ranks. J Fuel Chem Technol 43:129–137
72. Sabarish R, Unnikrishnan G (2018) PVA/PDADMAC/ZSM-5 zeolite hybrid matrix membranes for dye adsorption: fabrication, characterization, adsorption, kinetics and antimicrobial properties. J Environ Chem Eng 6(4):3860–3873